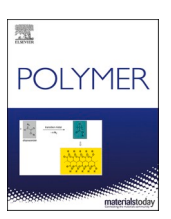


Contents lists available at ScienceDirect

Polymer

journal homepage: http://www.elsevier.com/locate/polymer





Synthesis of polymers in nanoreactors: A tool for manipulating polymer properties

Haoyu Zhao, Sindee L. Simon

Department of Chemical Engineering, Texas Tech University, Lubbock, TX, 79410, USA

ARTICLE INFO

Keywords:
Nanoconfinement
Polymerization reactions
Polymer properties

ABSTRACT

The use of nanoreactors to confine monomers and synthesize polymers results in changes in the reaction kinetics and polymer properties making nanoconfinement a potential tool for manipulating and engineering polymer properties. In this perspective, we cover conventional nanoconfinement hosts, nanopore-confined free radical, step-growth, and ring-opening polymerizations, and changes in molecular weight, tacticity, glass transition temperature (T_g) , thermal stability, and electrical properties. We use examples from research in our laboratory, as well as comparisons of the work in the literature, to illustrate the competing forces that drive these changes, namely molecular layering or orientation at the nanopore surface, decreased molecular and segmental diffusion, and catalytic or inhibitory effects caused by chemical moieties on the native or surface-functionalized nanopore surface. The majority of nanoconfined polymerizations are found to be accelerated, and in the case of free radical polymerizations to generally yield higher molecular weights and higher isotacticity. $T_g s$ for the nanoconfined polymers tend to increase if strong interactions exist between the polymer and the confinement surface, but depressions are observed for confined polycyanurates; the importance of removing unreacted monomer and comparing results to the bulk material of same molecular weight and structure is emphasized. Examples are also provided of enhanced thermal stability and conductivity of polymers synthesized under nanoconfinement.

1. Introduction

It is well known that the properties of materials change when they are confined to nanometer dimensions, i.e., to length scales less than approximately 100 nm. Considerable work has been performed in the last thirty years on the glass transition and related dynamics of nanoconfined glass-fromers, including low-molecular weight molecular glasses confined to nanopores [1-10] and polymeric glasses confined to ultrathin films [11-23], and a number of reviews have been written [24-28]. Less well studied is the influence of nanoconfined polymer synthesis on the reaction kinetics and properties of the polymer produced. In spite of this limited work, the history of nanoconfined polymerization goes back to Clasen who in 1956 [29] polymerized dimethyl butadiene clathrated within thiourea. Such polymerizations, generally known as inclusion polymerizations, are typically performed in the solid state, initiated by radiation, and have been used to produce stereoregular polymers, including all-trans poly(1,4 butadiene) produced in urea and thiourea hosts [30,31] and all-trans 3-methyl-1,4-pentadiene and poly((-)pinene) synthesized in deoxycholic acid crystals [32,33].

Isotacticity can also be enhanced, as in early polymerizations of dienes and methyl acrylonitrile synthesized in a cyclotriphosphazene [34,35] and more recently, 100% isotactic poly(acrylonitrile) was synthesized in urea [36]. Inclusion polymerization, albeit of interest in its own right, is not the focus of this perspective since the physics involved is driven by guest/host interactions and the crystal structure of the clathrated monomer. Rather, we focus on liquid-phase polymerizations and the changes in reaction kinetics and properties of the synthesized polymers that arise due to nanoconfinement effects.

The paper is organized as follows. First we review the characteristics of nanoconfinement media typically used for polymerization studies. We then discuss the influence of nanoconfinement on various different polymerization types and the properties of the produced polymers, including for free radical, pseudo-living radical, step-growth, and ring-opening polymerizations. We use our own work in these areas as illustrative examples to highlight important issues, as well as giving an overview of work in the field. We end with implications and a conclusion.

E-mail address: sindee.simon@ttu.edu (S.L. Simon).

^{*} Corresponding author.

2. Nanoconfinement media

The work in our own group on nanoconfined free radical and step growth polymerizations has been performed in the nanopores of controlled pore glass (CPG). These borosilicate glasses are produced by spinodal decomposition [37] and are available in a wide range of pore diameters ranging from 4 to 300 nm. The pore size is well controlled at \pm 10% from the mean, the matrix is stable with respect to organic liquids, and the pore surface can be functionalized to give "hydrophobic pores", for example, by converting the native silanol groups to trimethyl silyl [1]. CPG particles have a mesh size of 120/200 μm , and low molecular weight liquids imbibe easily and quickly, in a matter of seconds or minutes into the void volume by capillary forces. In addition, since the pore volume is generally above 50%, the CPG matrix is ideal for use in differential scanning calorimetry (DSC) studies because a sufficient amount of monomer can be loaded to give strong signals; in addition, heat transfer for DSC measurements of nanoconfined polymerizations is not an issue for typical reaction rates. CPG pores are tortuous and interconnected, and thus, the material has been said to give a confinement environment between 2D and 3D [26]. Other silica-based media that have been used for nanoconfinement studies, include sol-gel and xerogel monolithic glasses, such as Gelsil, which have small (<5 nm) inkwell-type pore interconnections that have been said to give 3D [38] or between 2D and 3D [26] confinement. Although these latter glasses can be used as confinement media for polymerizations, their monolithic character results in much longer length scales and times for imbibement, making them somewhat less practical than some of the other confinement media for polymerization studies. In addition, hybrid inorganic-organic mesoporous silicates system [39-41], including MCM-41 [42,43], and SBA-15 [44-47], which were originally developed as catalytic supports and have been used for catalytic polymerization of olefins and cyclic monomers [48-54], are also used as media to study nanoconfinements in the absence of catalysis. With their small ~ 3 nm cylindrical channels arranged in a hexagonal lattice with no pore channel intersection, mesoporous silica provides a 2D confinement environment; they also are known to have micropores but the relative volume of the larger pores is small compared to the nanochannels. Removal of synthesized polymer from all of these silicate glasses is typically accomplished by solvent extraction, making their use for large scale production untenable. However, understanding how nanoscale confinement, in the absence of additional catalyst, in these environments impacts polymerization and the resulting properties is anticipated to facilitate development of nanoreactors in which confinement size can be used as a synthetic tool to control properties.

Another popular confinement medium is porous anodized aluminum oxide (AAO), which is typically comprised of straight wall pores or channels that provide 2D confinement although more complex pore shapes can also be formed [55]. AAO membranes are available with pore sizes from 2.5 to 300 nm, porosity from 8 to 15%, and membrane thickness up to 100 μm . Due to their straight channels, AAO membranes can be used as matrices to follow reactions via spectroscopic techniques, but their low porosity limit their use for following polymerizations in-situ with DSC because multiple membranes must be well stacked to provide sufficient material and good heat transfer for a strong signal. On the other hand, thin AAO membranes ($\leq 10~\mu m$) can be used as a nanoconfinement matrix with Flash DSC [56], although issues with monomer volatility limits their use for in-situ polymerizations. The AAO template can be dissolved using sodium hydroxide or phosphoric acid to yield polymeric nanorods or nanowires.

Metallic organic frameworks (MOFs), also termed porous coordinating polymers (PCPs), have much smaller nanochannels that can be designed by changing the combination of metal ion and organic ligand [57]. Channels are typically 1 to 10 Å per side, with square, rectangular, or hexagonal shape, and can be isolated from one another resulting in 2D confinement or interconnected resulting in a percolated network and in a 3D confinement environment [58]. Because their size is commensurate

with the size of many monomers, reaction kinetics may change; for example, living polymerizations in the absence of termination may result, as discussed in more detail later. In addition, the PCP template can be removed by aqueous tetrasodium ethylenediaminetetraacetate to produce templated polymer nanoparticles and porous nanoparticles that retained the shape of the nanocavities [59].

3. Nanoconfined free radical polymerizations

3.1. Kinetics of n-alkyl methacrylate polymerization

The thermally-initiated free radical polymerizations of several nalkyl methacrylates and benzyl methacrylate nanoconfined in CPG have been studied in our group by differential scanning calorimetry (DSC) using 2,2'-azobis(2-methylpropionitrile) (AIBN) and di-tert-butyl peroxide (DtBP) as initiators [60-65]. In these systems, the nanoconfined reaction kinetics are significantly accelerated, as shown in Fig. 1 for methyl methacrylate reacted at various temperatures in bulk (open symbols) and in 13 nm-diameter "silanized" CPG (filled symbols) in which the surface silanol group is converted to trimethyl silyl. Although the initial rate of reaction, which is the slope in the conversion versus time plot, is essentially unchanged upon nanoconfinement for MMA in these silanized pores, the Tromsdorff effect or autoacceleration occurs much earlier, resulting in earlier completion of the nanoconfined reaction. Autoacceleration occurs in the bulk as viscosity increases leading to a decrease in chain diffusivity and a concomitant decrease in the rate of termination relative to propagation. Under nanoconfinement, chain diffusion is suppressed such that the onset of autoacceleration occurs at earlier conversions. We modeled this effect [61], as shown by the lines in Fig. 1, by extending the model of Verros et al. [66] to account for the diffusion-controlled termination at the nanoscale assuming that the diffusion coefficient scales with pore diameter to the 1.3 power and molecular weight to the -3 power, both consistent with simulations [67, 68]; the model well describes the experimental data using the parameters that fit the bulk data plus only one additional parameter, the scaling prefactor for diffusion, for all of the nanoconfined data (including in larger pores) suggesting that the pertinent physics are captured. In addition to this evidence that the mechanism of nanoconfined

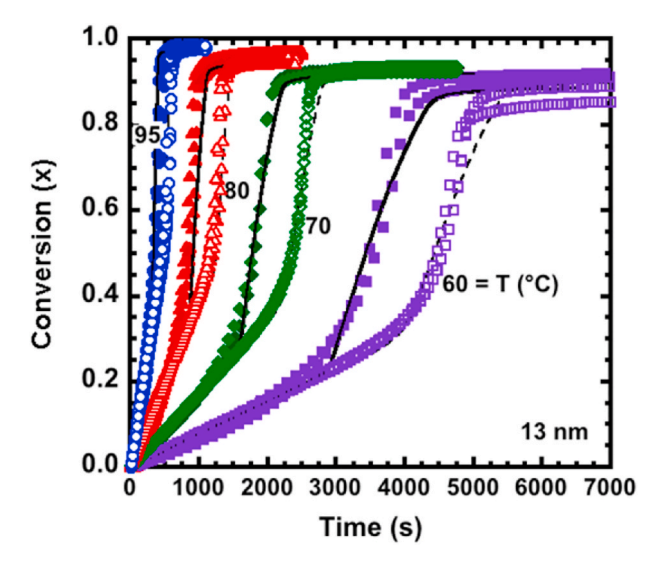


Fig. 1. Conversion vs time after induction for polymerization of MMA with AIBN initiator in bulk (open symbols) and in 13-nm diameter silanized CPG (filled symbols) at the temperatures indicated. The lines are model fits with solid lines indicating the fit to the nanoconfined case and the dashed lines to the bulk case. View in color for best clarity. Replotted after Begum, Zhao, and Simon [61]. (For interpretation of the references to color in this figure legend, the reader is referred to the Web version of this article.)

polymerization is the same as that of bulk free radical polymerization, we also find that the initial rate of nanoconfined free radical polymerization follows the expected scaling with initiator concentration to the 0.5 power [69].

The data shown in Fig. 1 are the polymerization of methyl methacrylate in hydrophobic silanized pores. The reaction was also performed in native hydrophilic pores, and for that case, the initial MMA reaction rate is faster than for either bulk or silanized pores due to the specific interactions between the monomer and the silanol groups on the pore surface; the increase scales linearly with reciprocal pore diameter indicating that the rate constant is proportional to the pore surface area to volume ratio, i.e., to the surface concentration of silanol groups [60].

For longer n-alkyl groups, the rates in both native and silanized nanopores increase relative to the bulk, as is shown in Fig. 2 for polymerizations of ethyl methacrylate (EMA) and butyl methacrylate (BMA) with DtBP initiator at 120 °C in bulk and in 8 nm-diameter CPG nanopores [63]. The increase in the initial rate in silanized pores seems to depend on the length of the n-alkyl group, increasing as the alkyl substituent increases in size, perhaps due to layering in the pores resulting in higher local concentration of monomer available to the growing chain end which seems to be oriented near the pore wall, as is discussed later. It is also observed that autoacceleration accelerates the reaction more in the EMA system than in the BMA system, consistent with the general finding that autoacceleration weakens as the n-alkyl group increases in size. Common wisdom explains this effect in terms of the T_{g} of the reaction system, with the lower Tgs associated with longer alkyl chains leading to lower viscosity and a less pronounced decrease in the termination rate as conversion increases. Interestingly, however, the onset of autoacceleration is found to occur at similar degrees of conversion for the ethyl- and butyl-methacrylate systems, and an analysis of the system T_g at the onset of autoacceleration indicates that the reaction mixtures are over 150 K above their Tg at this point, a regime in which the viscosity change is not strongly dependent on T-Tg [63]. That said, as the conversion increases after autoacceleration, the Tg also rapidly increases, and it increases to a greater extent in the higher T_g systems (i.e., those with shorter alkyl substituents), thus resulting in more dramatic increases in reaction rate for the EMA compared to BMA monomer as a result of autoacceleration.

3.2. Molecular weight in nanoconfinement free radical polymerizations

The faster rate of reaction and earlier onset of autoacceleration, the latter of which is attributed to a reduction in the rate of termination, have interesting implications for the molecular weight of polymers

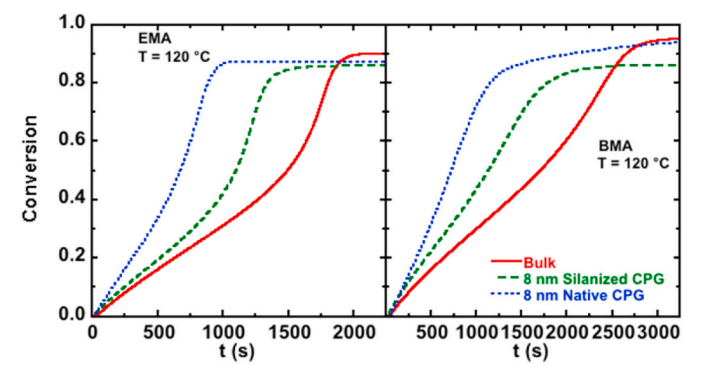


Fig. 2. Conversion vs time after induction for the thermally-initiated free radical polymerization for EMA (left) and BMA (right) at 120 °C with DTBP initiator for bulk (red solid line) and in 8-nm diameter silanized CPG (green dashed line) and 8-nm diameter native CPG (blue dotted line). View in color for best clarity. Reanalyzed based on data from Tian, Zhao, and Simon [63]. (For interpretation of the references to color in this figure legend, the reader is referred to the Web version of this article.)

synthesized under nanoconfinement. As we recall, molecular weight in conventional thermally initiated free radical polymerizations is determined by the relative rates of propagation and termination in the absence of chain breaking reactions. Hence, an earlier onset of autoacceleration results in higher molecular weights produced under nanoconfinement, and it also results in lower polydispersity at full conversion since more of the chains produced are the longer chains formed after autoacceleration [65]. In addition, if the rate of the reaction increases under nanoconfinement, as in the case of MMA in native pores or for EMA or BMA in either native or silanized pores, molecular weight will also increase due to the enhanced rate of propagation. The effects are clearly shown in GPC traces for the PMMA polymerized at 80 °C with AIBN initiator in Fig. 3, where the material synthesized in the native pores shows a monomodal peak eluting at the shortest times indicating the highest molecular weight and narrow polydispersity, whereas the material synthesized in the bulk elutes at the longest times and has a bimodal peak, indicating higher PDI, with the first (short time) peak attributed to chains synthesized after the onset of autoacceleration and the second (long time) shoulder attributed to the shorter chains produced at the initial stages of the reaction [65]. The GPC trace for the materials produced in the silanized CPG lies between those for the bulk and native pores with a smaller long-time shoulder compared to the bulk due to the earlier onset of autoacceleration.

Although the changes in molecular weight distribution for PMMA synthesized in CPG shown in Fig. 3 seems to be general, the details do depend on the type of confinement medium and the confinement size. A compilation of the data in the literature for PMMA is shown in Fig. 4, where the ratio of the nanoconfined number-average molecular weight (M_n) to that obtained in bulk polymerization is plotted as a function of nanoconfinement size on the left and the corresponding ratio for the polydispersity (PDI) is plotted on the right. In addition to our work in silanized and native CPG (open and filled red circles, respectively) [65], the results for PMMA synthesized in PCP [70], MCM-41,[71] SBA-15, [72] and Gelsil [73–75] are shown. The data shown are for thermally initiated free radical MMA polymerizations using AIBN initiator, or for

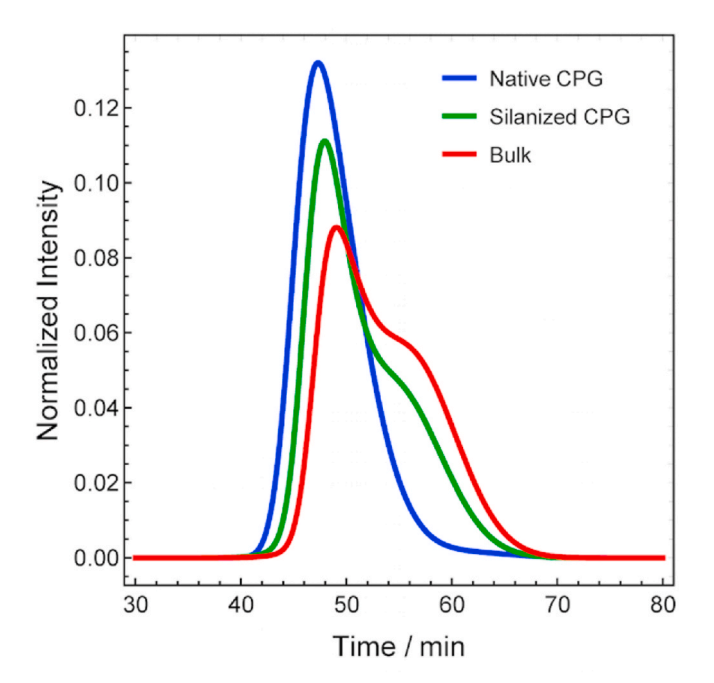


Fig. 3. GPC traces for PMMA synthesized at $80\,^{\circ}\text{C}$ with AIBN in bulk (red) and in $13\,$ nm-diameter silanized (green) and native (blue) CPG. Details of the polymerization can be found in Zhao et al. [65]. View in color for best clarity. (For interpretation of the references to color in this figure legend, the reader is referred to the Web version of this article.)

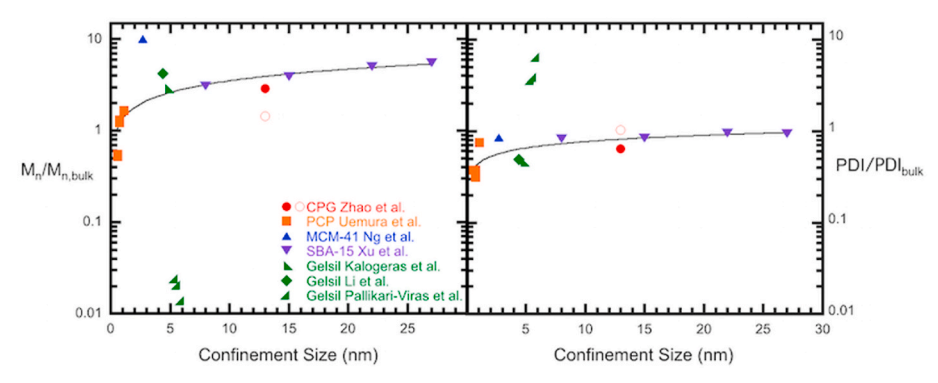


Fig. 4. Normalized number-average molecular weight (left) and normalized polydispersity (right) vs nanopore confinement size for PMMA synthesized under nanoconfinement. Data using AIBN as initiator for free radical polymerization include work from Zhao et al. [65] in native CPG (red filled circles) and in silanized CPG (red open circles); from Uemura et al. [70] in PCP (orange squares); and from Ng et al. [71] in MCM-41 (blue triangles). RAFT polymerization data is from by Xu et al. [72] in SBA-15 using AIBN initiator and a chain transfer agent (purple inverted triangles). Free radical polymerization data with BP as initiator in Gelsil are from Kalogeras et al. [73] (green left triangles), from Li et al. [74] (green diamonds), and from Pallikari-Viras et al. [75] (green right triangles). Lines are guides to eye only. View in color for best clarity. (For interpretation of the references to color in this figure legend, the reader is referred to the Web version of this article.)

the Gelsil work benzyl peroxide (BP) initiator, with the exception of the polymerizations in SBA-15 which are RAFT polymerizations using AIBN initiator and ethyl xanthate ethyl propionate as chain transfer agent. As shown, nanoconfinement of MMA typically results in an increase in the molecular weight of the PMMA produced ($M_n/M_{n,bulk}\,>\,1$) and a reduction of polydispersity ($PDI/PDI_{bulk} < 1$) with a sole exception of the work from Pallikari-Viras [75] which shows the opposite behavior for both M_n and PDI; the reason for this exception is unclear although, as they also noted, their earlier work by Li et al. [74] showed the more typical results. The molecular weight obtained in the MCM-41 by Ng et al. [71] was ten times that obtained in a bulk polymerization under the same conditions; the reaction was faster in the MCM-41 yielding full conversion in less than 2 h at 100 °C for the nanoconfined case compared to 86% conversion in the bulk case, but whether the large increase in M_n is simply the result of a faster rate of propagation or also due to an absence of termination leading to pseudo-living polymerizations in the small channels of the MCM-41 remains unanswered. The trend lines shown are simply guides to the eye, and of course, at large pore diameters (small degrees of confinement), the ratios will revert to M_n/M_n. _{bulk} = PDI/PDI_{bulk} = 1.0, thus, suggesting that a maximum may exist in the ratio of $M_n/M_{n,\text{bulk}}$. Also, of particular interest is that the PDI of the polymer produced was found to be as low as 1.6 for our MMA polymerizations in native 13-nm diameter CPG at full conversion [65]; Ng et al. found the similarly low value of 1.7 for MMA polymerization in MCM-41 and Kalogeras and Neagu found PDI of 1.2 for polymerization in Gelsil [73]. These values are much lower than for the corresponding bulk free radical polymerization at full conversion. Interestingly, values of PDI below 2.0 are unable to be captured by our model of nanoconfined MMA polymerization leading us to speculate that the rate of initiation may increase upon CPG nanoconfinement [65]; however, other works, for example by Uemura et al. [70] and Achilias and coworkers [76] have suggested that initiator efficiency may decrease in the very small nanopores of PCP for styrene polymerization and in the presence of graphene oxide for a methacrylate.

The increase in molecular weight and decrease in PDI observed for PMMA synthesized by free radical polymerization in nanopores is not easily generalized to the higher-order poly(n-alkyl methacrylates). Although the molecular weight obtained from nanoconfined polymerization of ethyl methacrylate in 8-nm diameter CPG is greater than the bulk, for longer alkyl chains, M_n decreases relative to that of the bulk. It is well known that autoacceleration is less dramatic as the n-alkyl group increases in size, as shown in the reaction kinetics for ethyl- and butyl-methacrylate monomers in Fig. 2, and thus, since the earlier onset of autoacceleration is one explanation for the increase in molecular weights from nanoconfined free radical polymerizations, the reduced gel effect with increasing size of the n-alkyl substituent may lead to smaller changes in molecular weight between bulk and nanoconfined

polymerizations, as is observed from methyl-to ethyl-methacrylate. However, a reduced gel effect should not lead to a decrease in molecular weight for nanoconfined polymerizations of monomers with longer alkyl groups relative to the bulk since the rates of the nanoconfined reactions are higher and autoacceleration, even if it is less dramatic, still may occur at earlier conversions under nanoconfinement. The explanation may lie in a decrease in chain transfer to the polymer under nanoconfinement for the case of the longer n-alkyl methacrylates. Demonstrating the effect, molecular weight data for poly(dodecyl methacrylate) (PDMA) synthesized in bulk and in 7.5 nm-diameter native CPG is shown in Fig. 5 in which the natural logarithm of the degree of polymerization is plotted versus reciprocal temperature [77]. As temperature decreases above the ceiling temperature of approximately 195 °C (i.e., as reciprocal temperature increases above 1000/T = 2.14 K⁻¹), the molecular weight produced in both bulk and nanoconfined reactions increases, with the bulk molecular weights increasing more rapidly. Chain transfer to polymer is known to increase with decreasing temperature in this system through attack of the alkyl group leading to branched and ultimately crosslinked networks [78-81]. Hence, at the lowest temperature investigated, of 120 °C, the bulk polymerization

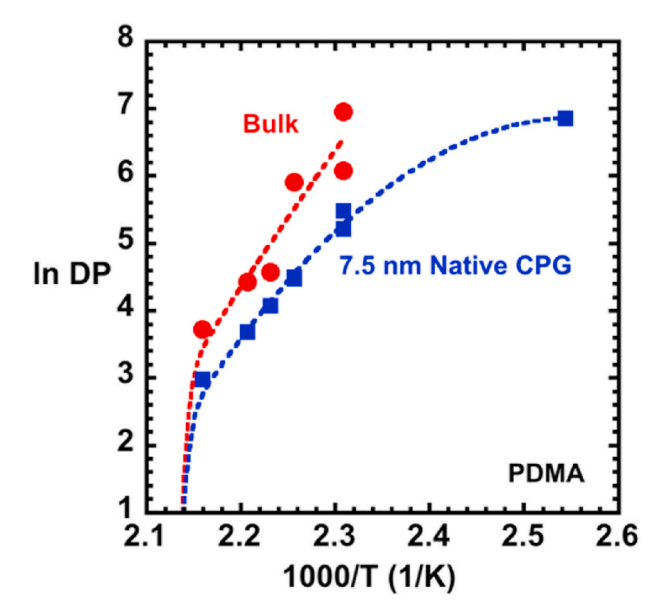


Fig. 5. Natural logarithm of the degree of polymerization vs reciprocal temperature for PDMA polymerized in bulk (red circles) and in 7.5 native CPG (blue squares) with 0.5% DtBP initiator. From Tian and Simon, [77]. (For interpretation of the references to color in this figure legend, the reader is referred to the Web version of this article.)

yields a crosslinked material of infinite molecular weight that is insoluble in solvent. On the other hand, the PDMA synthesized in 7.5 nm-diameter native CPG at all temperatures studied (down to $120\,^{\circ}\text{C}$) shows finite molecular weights that are lower than the bulk. We conclude that chain transfer to polymer in n-alkyl methacrylates is less prevalent under nanoconfinement due to the reduced diffusivity of polymer chains leading to a decrease in molecular weights relative to the bulk case for monomers with longer alkyl groups.

For the case of the benzyl methacrylate monomer, polymerization rate and molecular weight both increase relative to the bulk in 4 and 8 nm-diameter native CPG with 1.5% AIBN initiator similar to the cases of methyl and ethyl methacrylates, but increasing the initiator concentration to 2.5% AIBN results in a decrease of molecular weight relative to the bulk for polymerization in 4 nm CPG for an unknown reason; in addition, PDI is similar or higher than in the bulk [69]. Interestingly, autoacceleration seems to be suppressed in the nanoconfined benzyl methacrylate and this may account for some of the differences between the molecular weight distribution in bulk and nanoconfined polymerizations, but more work is needed to fully understand the effect of substituent group on the reaction kinetics and resulting properties of nanoconfined methacrylate polymerizations.

Free radical polymerization of styrene has been carried out by two research groups, that of Kitawaga using PCP as the confinement matrix with size scales ranging from 0.4 to 1.0 nm [70] and that of Mijangos using 35 nm-diameter AAO nanoporous templates [82]. For the PCP, the polystyrene produced depends on the nanochannel shape and size, with intermediate size channels giving higher molecular weight and lower PDI than bulk, whereas the smallest and largest nanochannels gave significantly lower molecular weights. For both styrene and MMA in PCP, molecular weight is generally related to the conversion (with one exception), and samples having conversion x > 70% have molecular weights greater than bulk. For this reason, and the facts that i) the observed maximum conversion depends on monomer loading and ii) block copolymers can be produced with the addition of a second monomer, it was concluded by Kitawaga and coworkers that the polymerization in PCP was a pseudo-living polymerization in which termination did not occur given the small sizes of the channels [70].

On the other hand, in work by Mijangos and coworkers on polystyrene in 35-nm AAO template [82], the initial rate of reaction was higher than the bulk but the molecular weight and the PDI were smaller. In fact, the polymer produced under nanoconfinement showed monomodal molecular weight distribution, whereas that produced in bulk conditions was bimodal with the primary GPC peak occurring at longer elution times (lower molecular weights) than for the nanoconfined sample. The data suggests that autoacceleration plays an important role for the bulk reaction, resulting in the bimodal distribution and a higher average molecular weight at full conversion, but why autoacceleration is suppressed in the nanoconfined styrene polymerization is unclear.

In order to further control the polymerization product of nanoconfined free radical reactions, Antonietti, Matyjaszewski, Schmidt and coworkers performed a type of reversible deactivation radical polymerization termed activators regenerated by electron transfer atom transfer radical polymerization (ARGET ATRP) in untreated and surface functionalized MOF nanopores [83]. The technique demonstrated PDI ≤ 1.4, similar to that observed in the bulk, with molecular weights that were three to four times higher for nanoconfined methyl-, ethyl-, and benzyl-methacrylate monomers. Moreover, grafting the initiator to the MOF surface further enhanced Mn to values as high as an order of magnitude greater than those in the bulk, with Mn being reciprocal to initiator graft density. In addition, similar to the findings of Uemura et al. in very small PCP [70], the nanoconfined polymerization is pseudo-living with molecular weight being dependent on the monomer loading in the pores and with the ability to make block copolymers on addition of a second monomer after the first has reacted. In the case of vinyl esters monomers synthesized in MOF by Schmidt and coworkers [84], polydispersity ranged from 1.5 for the vinyl butyrate to 2.2 for

vinyl acetate, with corresponding number-average molecular weights of 17,500 and 42,500 g/mol, respectively. Here, both PDI and molecular weight were much smaller than those obtained by bulk polymerization because chain transfer to polymer, which is very prevalent in the bulk, is presumed to be suppressed under nanoconfinement. The molecular weight, PDI, and conversion were all found to depend on monomer size, decreasing as monomer size increased, because of partial monomer loading in the nanochannels.

3.3. Tacticity in nanoconfined free radical polymerizations

Tacticity can also be strongly impacted by nanoconfinement. Conventionally, it is tuned by polymerization with metal catalysts (i.e., Ziegler-Natta catalysts) or alternatively reacted via living anionic polymerization [85] or free radical polymerization with fluoroalcohol [86,87] or Lewis acids additives [88,89]. Inclusion polymerization, in which the monomer is oriented and often forms a co-crystal in clathrates, can also give high tacticity as mentioned earlier [34,35]. In the case of nanoconfined liquid-state free radical polymerizations, both confinement size and the nature of interactions between the monomer and the pore surface appear to drive changes in tacticity. In our work on MMA free radical polymerization, isotacticity increased dramatically for the polymerizations in 13-nm diameter native CPG, as shown in Fig. 6, where the percentage of isotactic triads (mm) and the enhancement of mesodiads (m) are plotted as a function of reaction temperature for bulk and nanopore confined polymerizations [65]. The percentage of isotactic triads increased from 12% in bulk polymerization at 95 °C to 52% in the nanoconfined case, whereas the percent of mesodiads increased from 29% to 61%. These are very significant changes and indicate that the combination of surface interactions and nanoconfinement, in which the less sterically bulky isotactic structure is more favorable than the more sterically hindered syndiotactic structure, can profoundly influence tacticity.

Although the nanoporous host provides a physical means to tune the stereoregularity of vinyl monomers, the results vary significantly depending on the type of confinement matrix, as shown by a compilation of the literature results in Fig. 7 for the isotacticity of PMMA synthesized under nanoconfinement. In general, smaller pore sizes tend to produce higher isotacticity content due to the more confined environment

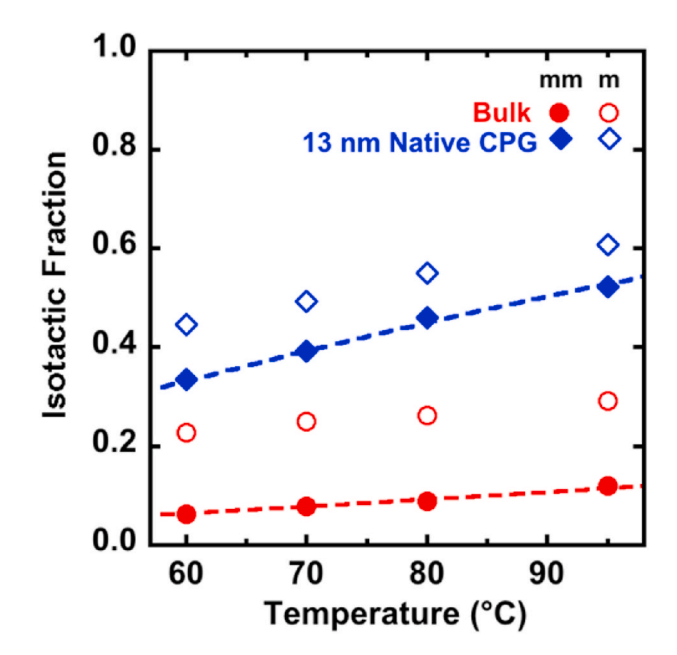


Fig. 6. Isotactic triads (mm) and mesodiads (m) as a function of polymerization temperature for PMMA synthesized in 13-nm diameter native CPG. After Zhao et al. [65].

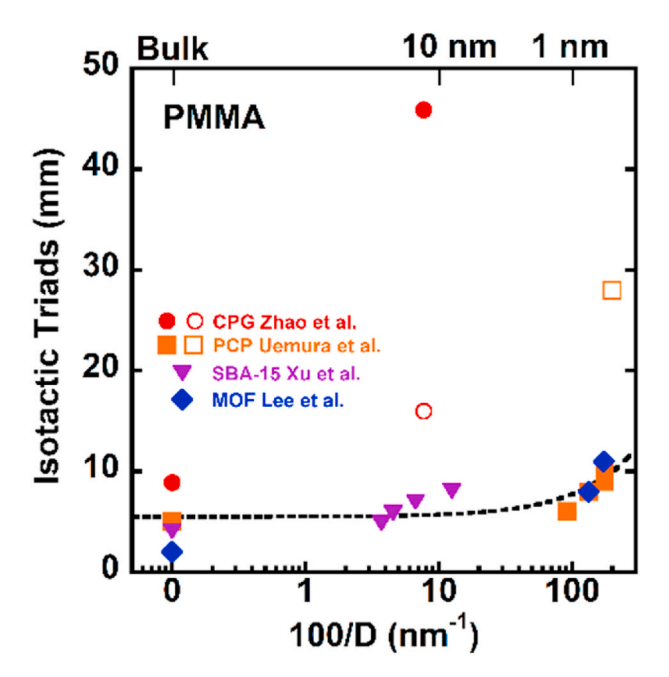


Fig. 7. Isotactic triads vs reciprocal pore size for bulk and nanoconfined PMMA for various matrices and for pore sizes ranging from 0.5 to 30 nm. Data using AIBN as initiator for free radical polymerization include work from Zhao et al. [65] in native CPG (red filled circles) and in silanized CPG (red open circles); from Uemura et al. [70] in PCP (orange filled squares); and from Uemura et al. [90] in helically twisted PCP (orange open squares). RAFT polymerization data is from by Xu et al. [72] in SBA-15 using AIBN initiator and a chain transfer agent (purple inverted triangles). ATRP polymerization is from Lee et al. in inert or surface-grafted MOF [83] (blue filled diamonds). Line is a guide to eye only. View in color for best clarity. (For interpretation of the references to color in this figure legend, the reader is referred to the Web version of this article.)

favoring the isotactic structure; however, the enhancement for MMA synthesized under mesoporous silicates SBA-15 [72] is minimal except at the smallest pores where isotacticity is enhanced by nearly a factor of two relative to the bulk value, which we suggest is an intrinsic size effect without the influence of specific interactions orienting the growing chain. Similarly, MOF hosts include extremely small channels (<1 nm), but the improvement in isotacticity is still limited even for surface functionalized MOF [83]. In fact, only in two cases are dramatic increases in isotacticity observed for PMMA synthesized under nanoconfinement: one is in our 13 nm hydrophilic CPG pores [65] and the other is in highly helically twisted PCP channels that are considerably smaller at $4 \times 7 \text{ Å}^2$ [90]. The advantage of the CPG is due to its relatively large size, it can be completely filled and the reaction goes to completion; on the other hand, in the case of the helically twisted PCP channel, only 42% conversion and relatively low molecular weight was achieved although the channel does obviously facilitate the growth of isotactic

In general, for vinyl monomers, stereoregularity correlates with the steric demands of the side group. A compilation of the increase in isotactic triads over bulk (mmconfined – mmbulk) is shown for various vinyl monomers in Fig. 8 as a function of reciprocal confinement pores size. Comparing the n-alkyl methacrylate monomers polymerized in MOFs [83], including methyl-, ethyl-, and benzyl-methacrylate (MMA, EMA, and BZMA, respectively), reveals that the isotacticity for PMMA and PEMA increases in untreated MOF, and an even greater enhancement is observed in MOF having initiator grafted to the pore surface, presumably because the initiator at the pore surface orients the chain end at the wall and restricts the approach of incoming monomers. In the case of the MOF polymerizations of vinyl acetate (VAc), vinyl propionate (VPr), and vinyl butyrate (VBu), via free radical polymerization, the polymers show an increase in isotacticity ranging from 5 to 14% over

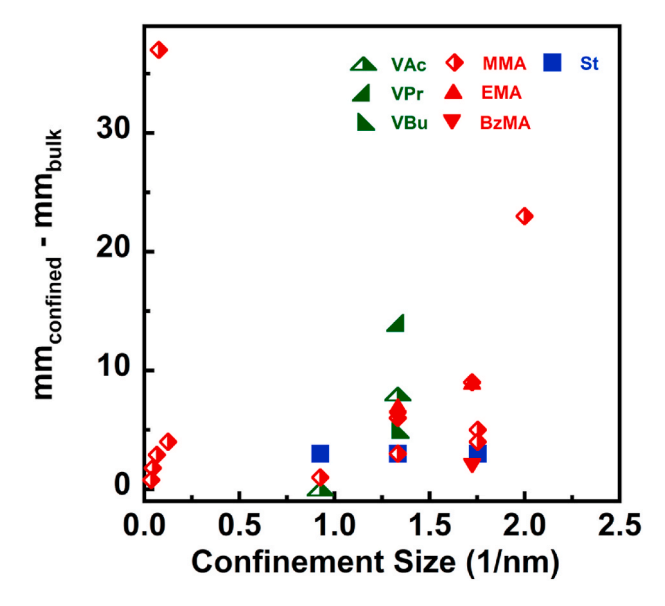


Fig. 8. Enhanced isotactic triads (mm_{confined} - mm_{bulk}) as a function of reciprocal nanopore size for vinyl monomers, green data representing vinyl esters [70,84] via ATRP under inert or surface-modified MOF, red data representing alkyl methacrylates [65,70,83,90] via free radical polymerization under MOF and CPG, and blue data representing styrene [70] via free radical polymerization under MOF. (For interpretation of the references to color in this figure legend, the reader is referred to the Web version of this article.)

that of bulk (\sim 20%), with the improvement influenced by the substituent group size and the mesodiads showing the highest isotacticity for nanoconfined PVPr [84].

In contrast to the case of isotactic triads, syndiotactic triads provide more space for the substituent, such that bulkier or more rigid moieties favor syndiotactic placement and lead to lower isotactic content. Examples are PBzMA [83], which contains 4% isotactic triads in modified MOF versus 2% in bulk, as compared to PMMA which has a much smaller substituent and 11% isotactic triads in the same MOF versus 2% in bulk. Another example is PVBu [84], which contains 25% isotactic triads in inert MOF versus 20% in bulk, as compared to PVAc which has a much smaller substituent and which contains 30% isotactic triads in the same MOF versus 22% in bulk. Furthermore, for the relatively bulky substituent of styrene polymerized in 35 nm AAO [82], a pentads analysis reveals that stereoregularity is shifted towards syndiotactic placement, with the syndiotactic peak having a value of 3.81 for the nanoconfined polymerization and a value of 1.38 for bulk polymerization, with a value of 5.9 expected for 100% syndiotactic material. On the other hand, at much higher nanoconfinement, PS shows a 3% increase in isotactic triads for polymerization in PCP having a pore size of 0.57 nm [70]. Thus, nanoconfinement can be used to tune tacticity but the results depend on the monomer and the confinement size, type, and surface chemistry.

4. Nanoconfined step growth polymerizations

For step growth polymerizations, the first investigation to examine the influence of nanoconfinement was performed by Amanuel and Malhorta [91] who found changes in the reactivity of phenolic resins in nanoporous silica. Motivated by those results, we undertook a series of investigations examining nanoconfined trimerization of cyanate esters [92–97]. We have found that the difunctional monomer bisphenol M dicyanate, which trimerizes to form a thermosetting polycyanurate, reacts some 20–30 times faster in 11.5 nm-diameter hydrophobic silanized pores relative to the bulk and 35–40 times faster in native hydrophilic pores, as shown in Fig. 9 [96,97]. Even larger enhancements are found for the reaction of a monofunctional cyanate ester,

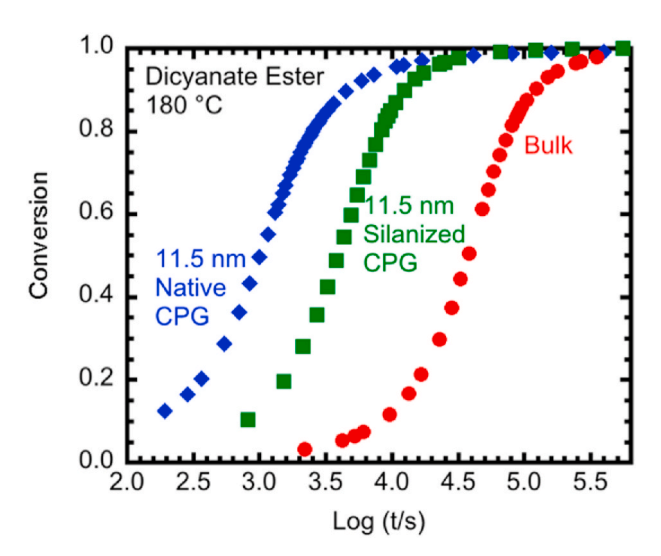


Fig. 9. Conversion vs log t for trimerization of bisphenol M dicyanate at $180\,^{\circ}$ C in bulk and in 11.5 nm-diameter hydrophobic and native CPG pores. Data after ref. Li and Simon [96,97].

4-cumylphenol cyanate, which produces a low-molecular-weight trimer reaction product: the monofunctional cyanate ester reacts approximately 50 times faster in 13 nm-diameter hydrophobic pores relative to the bulk [94], as shown in Fig. 10, indicating that the enhanced reactivity is not due to the polymeric nature of the reaction nor due to cyclization side reactions. No change in the activation energy is observed for either nanoconfined reaction. Furthermore, quantitatively similar increases in reactivity for both the mono- and di-functional cyanate ester are observed near the pore wall and in the center of the nanopores, based on the evolution of the glass transition temperature associated with the wall and that associated with the center of the pore, coupled with no changes in activation energy for the nanoconfined reactions; this precludes attribution of enhancements solely to catalysis at the wall by the silanol groups in native pores, even though these are known to promote the trimerization reaction [98].

Our initial hypothesis was that a smaller, more flexible monomer, such as the monocyanate ester, would need to be confined in smaller pores in order to experience the same degree of confinement and the same acceleration of reaction as experienced by a larger stiffer monomer. This was clearly not the case and warranted further investigation,

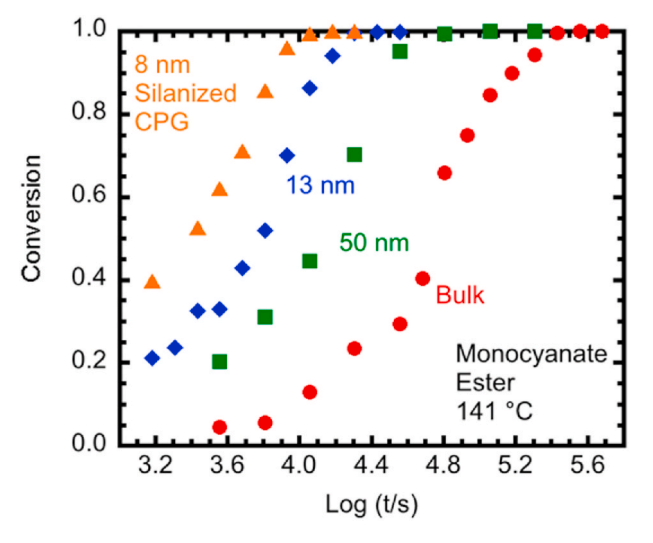


Fig. 10. Conversion vs log t for 4-cumylphenol cyanate at $141\,^{\circ}$ C in bulk and in hydrophobic CPGs of 8, 13, and 50 nm in diameter. Data after Koh and Simon [94].

and in particular, evaluation of the hypothesis that increases in local concentration due to changes in liquid structure or layering near the walls are responsible for enhanced reactivity. Lattice Monte Carlo (MC) simulations by Malvadi and coworkers on nanoconfined linear step polymerizations indicate that such changes in liquid structure compete with decreases in diffusivity such that reaction collisions and polymerization rates can be either accelerated or reduced at the nanoscale depending on which effect dominates [99]. On the other hand, molecular dynamics (MD) simulations for a nanoconfined epoxy/amine thermosetting polymerization indicated that no reactions took place near the walls and that, as a consequence, the reaction rate should be slower in the pores [100]. In order to examine the influence of the monomer structure and rate at the pore wall, we set out to purposefully disrupt order by using a mixture of mono- and di-cyanate ester. As shown in Fig. 11, when the phenyl moiety is assumed to preferentially interact with the wall, the layering of the monomers results in the cyanate ester function groups pointing away from the wall in a layer. For the monofunctional monomer, the cyanate ester functional groups lie in a single plane and their local concentration is higher than in the isotropic case, consistent with its higher reactivity. On the other hand, for the difunctional monomer, the layering is somewhat more uneven because of its more bulky structure. A mixture of the two monomers is expected to result in even worse layering. Indeed, a reduction of the acceleration of the reaction rate is observed under nanoconfinement as shown in Fig. 12, where the DSC heat flows for reaction during a dynamic temperature scan is shown for mono- and di-cyanate ester at top in 13 and 11-nm diameter CPG; the distance between the dashed lines for the nanoconfined reaction and the solid lines for the bulk reaction reflects the enhancement of the reaction rate. The lower figure shows the same comparison but for the mixed system in 8.1 nm diameter CPG; in spite of the smaller pore size, the reaction of the mixed monomer system is considerably less enhanced than in the two pure systems. Quantitatively, the rate constant increased by 12 times for the monomer mixture in 8.1 nm CPG, less than half the increase observed for the individual monomers in the pure state [92]. Thus, the enhanced reactivity in these systems is consistent with a higher concentration of functional groups as a result of layering at the pore wall following the arguments of Malvadi

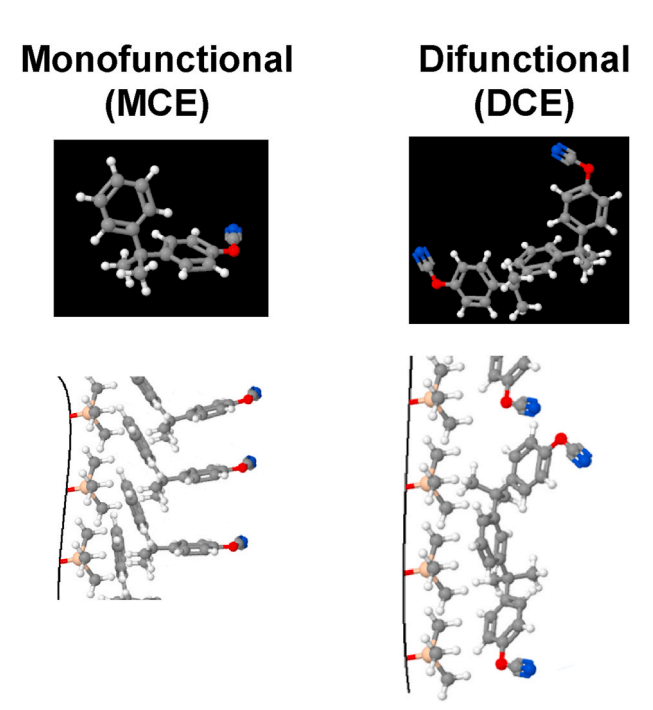


Fig. 11. Structure of the monocyanate ester (left) and dicyanate ester (right) and cartoon of potential layer near the wall assuming that the phenyl groups lie parallel to the surface.

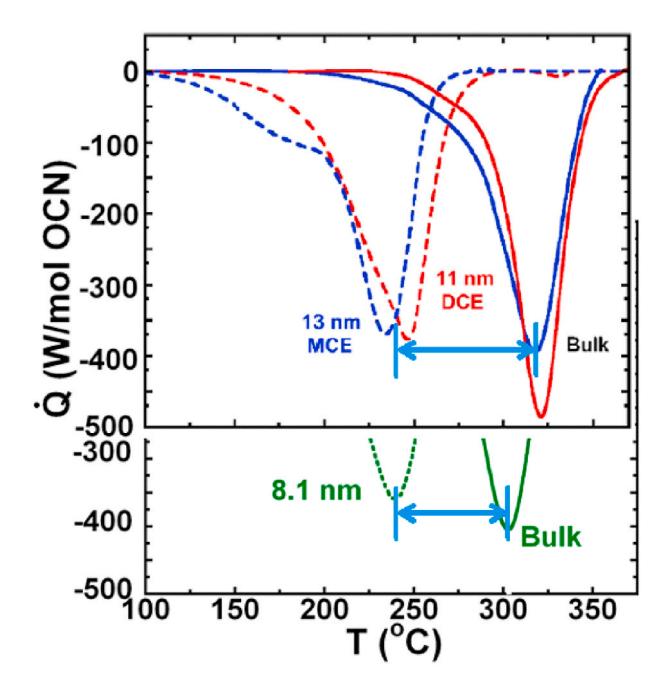


Fig. 12. DSC heat flow, with exotherm down, during a dynamic temperature ramp at 10 K/min. At top: mono- (blue) and di-(red) cyanate ester in 13 and 11-nm diameter CPG confinement, respectively, (dashed lines) and in bulk (solid lines). The distance between the peaks is a measure of the enhanced acceleration of the nanoconfined reaction. At bottom: 50/50 mixture of mono- and dicyanate ester in 8.1 nm-diameter CPG (green dashed line) and in bulk (green solid line). After Lopez and Simon [92] and Koh, Li, and Simon [95]. (For interpretation of the references to color in this figure legend, the reader is referred to the Web version of this article.)

and coworkers [99]. Layering at the surface or the opposite, i.e., disordering, was similarly used by Yancey and Vyazovkin to explain changes in the reaction rate in other cyanate ester systems; for example, in the solid state trimerization of sodium dicyanamide in nanoporous silica gel having surface silanol groups replaced by trimethyl silyl, a dramatic decrease in the nanoconfined reaction rate was attributed to the disordered layering of the crystalline monomer in the nanopores [101], whereas the acceleration of the nanoconfined reaction for small-molecule liquid state trimerizations in the same hydrophobic silica gel was attributed to layering at the pore wall [102].

The nanoconfined step-growth reaction between epoxide and aniline to give a linear polymer has been investigated by Paluch and coworkers using AAO confinement [103], and similar to the nanoconfined cyanate ester reaction, it shows an enhanced reaction rate, in this case by approximately a factor of 8 in 35 nm-diameter pores, and no change in activation energy. In the largest pores, the reaction slows down at the pore surface and the authors attribute this to the slower dynamics at the pore wall surface due to attractive interactions, but in the smallest 35 nm pores, the reactions at the pore wall and in the center of the pore show similar rates. The authors also note that nanoconfined reaction loses the autocatalytic nature that is observed in the bulk. A similar effect is observed for the dicyanate ester in the native CPG pores, as shown in Fig. 9, where the conversion versus time curve does not increase in slope as conversion increases to the same extent as it does for the silanized pores and bulk. The reason for this loss of autocatalytic character in our system, and presumably the reason for the loss in Paluch's work, is because the confined reaction is dominated by external catalysis, which in the case of the native CPG is due to silanol groups on the pore surface. This effect can be shown mathematically, writing the general reaction rate expression for epoxide reactions in terms of the change in conversion with time (dx/dt):

$$\frac{dx}{dt} = k(1-x)^n(x+b) \tag{1}$$

where k is the rate constant, n is the order of the reaction, and the term \mathbf{x} + b accounts for auto- and external catalysis. For bulk DGEBA epoxy, the external catalysis arises from impurities in the resin and the b value is typically less than 0.1,[104,105] such that the autocatalytic nature is very apparent as conversion increases. The loss of autocatalytic character in the case of the epoxy/aniline reaction in AAO is, thus, suggested by us to be attributable to catalysis by the AAO's hydroxylated surface, which has been shown to form readily at ambient temperatures and be difficult to remove [106-109].

The importance of catalysis by the AAO surface was recognized by Mijangos and coworkers in their work on the nanoconfined step-growth polymerization of triethylene glycol and hexamethylenediisocyanate to form polyurethane in AAO confinement [110]. The reaction rate increased as pore size was reduced at all confinement sizes, with acceleration over the bulk case by a factor of approximately three at 140 nm and by a factor of approximately ten at 35 nm. Not only was the enhancement attributed to catalysis by the hydroxyl groups on the alumina pore surface, but it was also modeled and well described using a surface concentration of 19.3 OH groups/nm², as reported in the literature [106]. In addition to the increase in reactivity, the molecular weight and PDI were substantially reduced, from M_n = 39,000 g/mol and PDI = 2.3 in the bulk to M_n of 7800 at 140 nm and 5000 at 35 nm and PDIs from 1.1 to 1.3 under nanoconfinement. This effect was attributed to a reduction in chain diffusivity at high conversion, hindering the ability of oligomers to combine to form larger molecules.

5. Nanoconfined ring-opening polymerization

For the majority of free radical and step growth polymerizations, nanoconfined polymerization is faster than that in the bulk due to several primary factors: specific interactions at the pore surface, higher local concentration of functional groups due to monomer layering at the pore surface, and, only in the case of free radical mechanism, a slowing down of chain diffusion that results in a slowing down of the termination step. Although the induction time becomes longer in nanoconfined free radical polymerization [60,63], the reason for which is not yet understood, the polymerization, once it starts, is seldom slower than in the bulk. In the case of ring-opening metathesis polymerization (ROMP) of dicyclopentadiene (DCPD) with second-generation Grubbs' catalyst investigated in our laboratory, however, the nanoconfined reaction presents very different behavior [111], as shown in Fig. 13 for the dynamic reaction at 10 K/min in differential scanning calorimetry (DSC). The bulk reaction (in red) shows the typical exotherm with an onset around 50 °C and a peak near 70 °C. For the reaction confined to 110 nm-diameter CPG, the onset of the polymerization exotherm occurs at a higher temperature indicating a reduced initial reaction rate under nanoconfinement. Perhaps even more interesting, the nanoconfined sample only undergoes a limited amount of polymerization as indicated by the decreased size of the exotherm (which is normalized to the mass of the sample) before the reverse Diels-Alder reaction sets in, the latter of which converts the dicyclopentadiene monomer to cyclopentadiene. The reverse Diels-Alder does not occur in the catalyzed bulk system. Its presence in the catalyzed nanoconfined system appears to be due to an acceleration of the reverse Diels-Alder reaction under nanoconfinement coupled with a decrease in the rate of polymerization. As Malvadi indicated in their analysis for step-growth reactions, the rate of reaction can increase due to higher local concentration of monomer or decrease due to diffusion effects. However, diffusion of monomer is very fast at typical reaction temperatures (which are far above the T_g of the monomer) even in a nanoconfined environment, and it is only if the reaction occurs on a similar timescale as diffusion will the rate be impacted; in other words, after Rabinowitch [112], the observed rate of

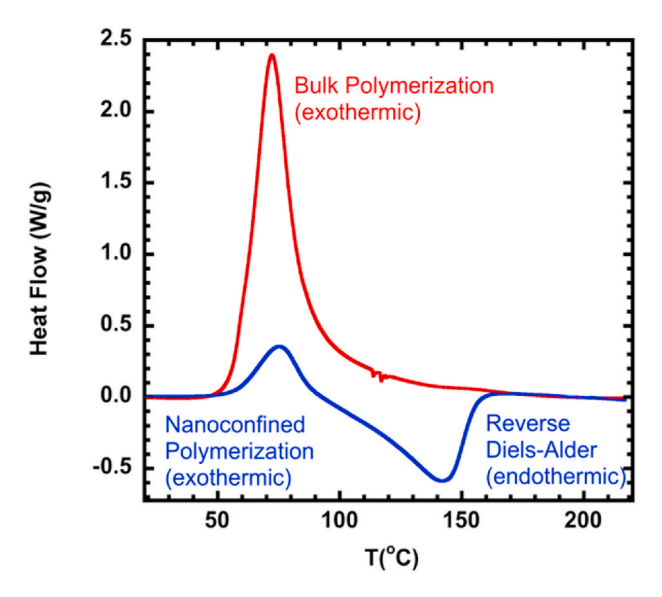


Fig. 13. DSC heat flow vs temperature for dicyclopentadiene undergoing ROMP reaction in bulk (red) during a dynamic scan at 10 K/min, and for the monomer in 110 nm-diameter CPG pores (blue). The exothermic direction is upwards (positive heat flow). View in color for optimal clarity. After Vaddey and Simon [111] (For interpretation of the references to color in this figure legend, the reader is referred to the Web version of this article.)

$$\frac{1}{k_{abs}} = \frac{1}{k_{intr}} + t_{diff} \tag{2}$$

reaction, k_{obs} , is reciprocally related to the sum of the timescale for diffusion, t_{diff} , and the intrinsic time scale of the reaction (1/ k_{intr}):

Hence, it is only because the ROMP reaction is very fast, reaching 90% conversion in less than 1 min during the heating scan that the time scale of monomer diffusion becomes relevant. To the best of our knowledge, this is the first demonstration of a secondary reaction competing with polymerization under nanoconfined conditions to yield a product not obtained in conventional unconfined conditions. An analogous result was found by Vyazovkin and coworkers for degradation of polystyrene-grafted clay nanocomposites, where the product α -methyl styrene was obtained in high yield for the nanocomposite but not for bulk polystyrene degradation, presumably due to an increased amount of intermolecular radical transfer resulting from the grafted chain structure [113].

A much slower ring-opening reaction, that of caprolactone to make nylon 6, was studied by Paluch and coworkers using AAO templates with pore diameters from 35 to 150 nm as the confinement media [114], and perhaps not unexpectedly, their results show that the nanoconfined polymerization is faster than the bulk, giving much higher conversions after a set reaction time (60 min at 80 $^{\circ}$ C), as well as higher molecular weight and lower polydispersity. In fact, molecular weights increased by up to a factor of four, with chains of 53,000 g/mol produced. Interestingly, the molecular weight of the nanopolymerized polycaprolacone was found to be independent of pore size for both reactions with and without water, which is contrary to most of the previously discussed experimental observations regarding free radical or step polymerization under confinement. The enhanced molecular weight and reduced PDI appear to be related to the suppression of side reactions, namely hydrolysis and backbiting reactions, yielding a monomodal polymer product.

6. Nanoconfined polymerization and the glass transition temperature

As mentioned in the introduction, a significant amount of work has been performed in the last thirty years on the glass transition and related dynamics, for molecular glasses in pores [1-10] and polymeric glasses confined to ultrathin films [11-23], and a number of reviews have been written [24–28]. The glass transition of ultrathin polymers has been found to decrease, increase, or remain unchanged, depending on the polymer, its molecular weight, the presence of small molecule plasticizers or antiplasticizers, and the interactions with the substrate. The leading explanation in the polymer community is that depressions in T_g relative to the bulk arise from enhanced mobility associated with the free surface, whereas increases in Tg arise from reductions in mobility associated with interactions with a strongly attracting substrate, with both free surface and substrate leading to large gradients in mobility throughout the thin film [16,25,115-128]. Reports of the existence of two distinct, albeit broad, Tgs in ultrathin films lends even more credibility to these arguments [115–117]. However, in seeming contradiction to the thin film results, nanopore-confined glasses in matrices without strong attractions also often show the existence of two T_os in spite of the lack of a free surface: a primary transition (Tg1) which is usually depressed relative to the bulk and a secondary transition (Tg2) which is often 15-30 K higher than the primary Tg and may or may not be higher than the bulk. Since the relative magnitudes of the primary and secondary transitions (in terms of the step change in heat capacity at Tg) decrease with decreasing nanopore size, researchers have associated the primary transition with material at the center of the pore and the secondary T_{σ} with material at the surface of the pore [4–9]. An example is shown in Fig. 14 for the cyanurate trimer (whose reaction kinetics were shown in Fig. 9) that was synthesized in bulk and in 13 nm-diameter silanized CPG pores [93]. Two T_gs are observed for the nanoconfined sample, both of which are lower than the bulk, and for this case, we corroborated the value of the Tg depression obtained for material synthesized in the nanopores by also synthesizing the material outside the pores and imbibing it into the pores, obtaining the same Tg values within 2 and 4 K for Tg1 and Tg2, respectively. The presence of two Tgs for the polycyanurate synthesized in 24-nm diameter native pores (whose reaction was shown in Fig. 8) are similarly shown in Fig. 15; for this material, also, both $T_{\rm g}s$, when they are discernable, are below the bulk values [96]. The dependence of the Tg depression on confinement size is

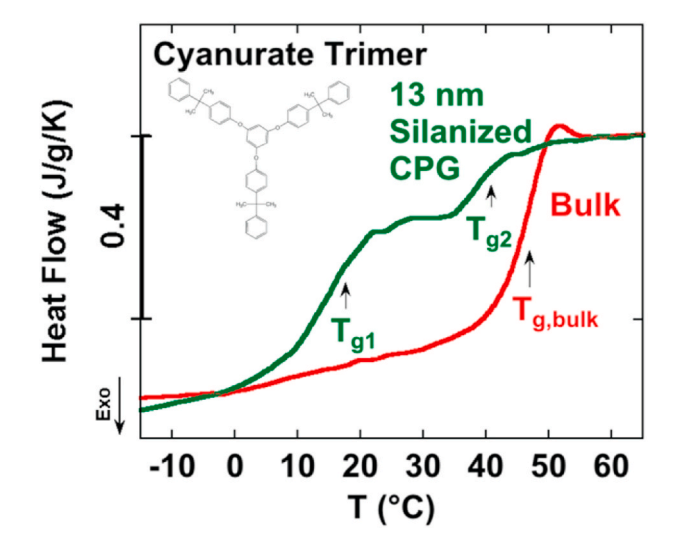


Fig. 14. DSC heat flow vs temperature showing T_g s for cyanurate trimer synthesized in bulk (red) and in 13-nm diameter silanized CPG pores (green). The structure of the trimer is shown in the inset. After Koh and Simon [93]. (For interpretation of the references to color in this figure legend, the reader is referred to the Web version of this article.)

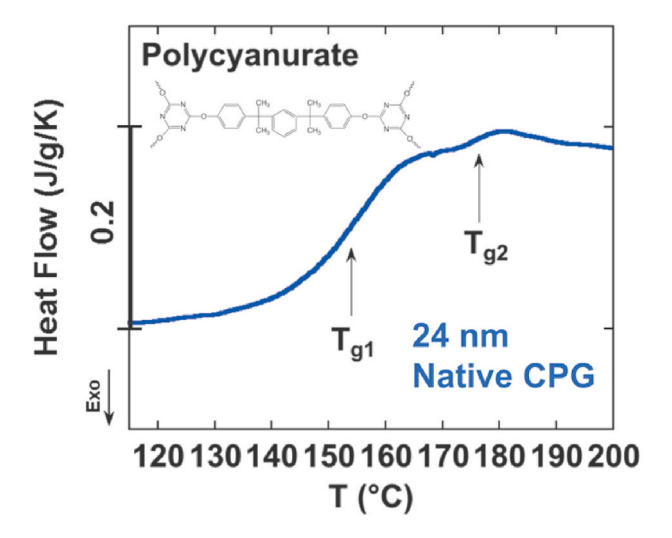


Fig. 15. DSC heat flow vs temperature showing T_gs for polycyanurate synthesized in 24-nm diameter native CPG pores. The two Tgs are marked, and the structure of the crosslinked material is shown in the inset. After Li and Simon[96].

shown in Fig. 16 for the primary T_{g1} of the polycyanurate where the change in Tg is plotted as a function of reciprocal nanopore diameter at 0, 33, 66, and 100% conversion. The confined monomer (0% conversion) shows little or no change in T_g on confinement, whereas the fully reacted material shows the largest change. Also shown in this figure is the difference between the T_g values in native and silanized pores as filled and open symbols, respectively; in general, the two are within a few K of one another, except in 24.6 nm pores at 100% conversion, where the native sample shows two Tgs and the silanized sample displays only one that is 20 K higher, closer to $T_{\rm g2}$ of the native sample than T_{g1} . However, when both T_{g8} are present, the T_{g1} and T_{g2} values are generally very similar, independent of pore surface chemistry. As mentioned, one can estimate the size of the surface layer associated with the secondary T_{g2}, and it is found to be 1.2 nm for the cyanurate trimer and 0.9 nm for the polycyanurate [94,96]. Similar length scales for the surface layer have been reported in the literature for

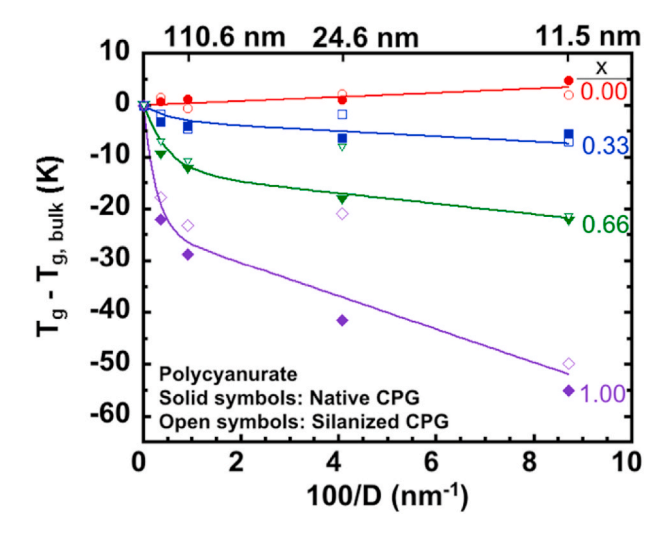


Fig. 16. Change in T_g from the bulk value vs reciprocal pore diameter for nanoconfined dicyanate ester/polycynaurate system as a function of conversion at conversions of 0 (red circles), 33 (blue squares), 66 (green triangles), and 100% (purple diamonds). Solid symbols are for material in native CPG and open symbols are in silanized CPG. Lines are a guide to eye only. After Li and Simon [96]. (For interpretation of the references to color in this figure legend, the reader is referred to the Web version of this article.)

polystyrene/o-terphenyl [4], although glycerol and propylene glycol in Gelsil give a length scale of 0.15 nm [5]. In addition, a three-layer model for various hydrogen-bonded liquids gives length scales between 0.3 and 0.9 nm [9].

Although studies of the Tg of materials synthesized in nanopores add another dimension to the large body literature on Tg and confinement effects, the results must be taken with a few caveats as alluded to in the previous discussion. First and foremost, it is typically not enough to compare the Tg of the polymer synthesized under nanoconfinement to that of the polymer synthesized in the bulk unless care is taken to ensure that the materials are identical, because, as has been shown in the previous sections, the molecular weight, PDI, conversion, and tacticity of the material synthesized under nanoconfinement may differ dramatically from that synthesized in the bulk. We note that in the case of the trimerization step-growth reactions, we demonstrated that full conversion was reached in the pores and that the structure of the polycyanurate network did not appear to change from the bulk, for example having the same conversion at gelation and the same normalized Tg vs conversion relationship [96,97]. However, if this were not the case, the nanoconfined material should be compared to itself after extraction from confinement. In addition, as alluded to, full conversion must be ensured or, if not, the residual monomer must be removed prior to T_o measurement of the nanoconfined sample; otherwise, one risks observing a depressed Tg due to plasticization of unreacted monomer. Fig. 17 exemplifies data for PMMA where these issues have been addressed [65]. The Tgs of the material in bulk and in nanopores (solid curves) are measured after removal of monomer using a pinhole and performing multiple heating ramps to 180 °C in order to evaporate any residual MMA. For the bulk sample, this pinhole method gave a similar Tg value to that obtained using the extraction procedure with ethyl acetate and then drying for 24 h at 80 °C in a vacuum oven. This same extraction procedure was used to get the material out of the nanopores with hydroquinone added to quench any active radicals. The results in Fig. 17 demonstrate that T_g is elevated 8 K in silanized pores and 12 K in native pores (both relative to the extracted material), consistent with the similarly small differences between silanized and native pores in Fig. 16

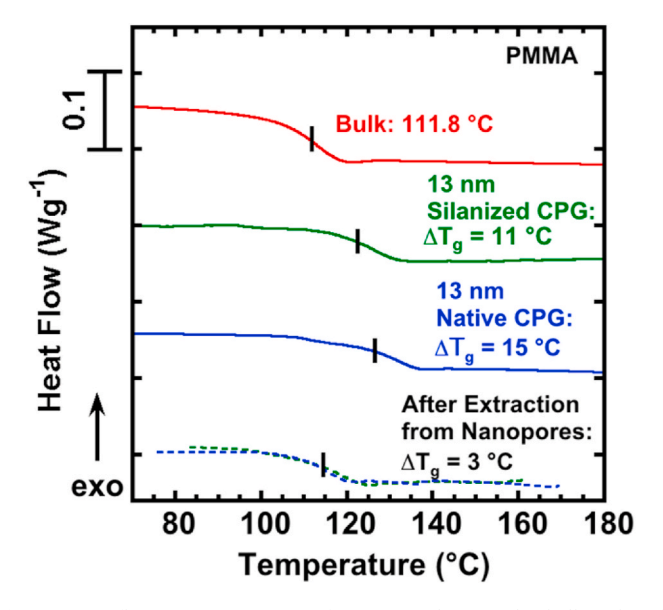


Fig. 17. Heat flow versus temperature for PMMA polymerized in bulk (red) and synthesized under nanoconfined conditions at 80 $^{\circ}$ C in 13 nm-diameter silanized (green) and native (blue) pores. The dashed lines and solid lines represent samples after extraction and after unreacted MMA removal, respectively. The vertical tick mark indicates the glass transition temperature. View in color for increased clarity. After Zhao and Simon [65]. (For interpretation of the references to color in this figure legend, the reader is referred to the Web version of this article.)

for the dicyanate ester/polycyanurate system. Had the nanoconfined material been compared directly with the bulk, values would be erroneously higher by 3 K, and if the residual monomer had not been extracted, an additional error of 16 K (higher) would have been observed in the case of the hydrophilic pores based on the Fox equation because the conversion was 98% in native pores and only 95% in the bulk. Although in this case, the conclusions that $T_{\rm g}$ increases for PMMA confined to nanopores would not change, the magnitude of the $T_{\rm g}$ elevation can be significantly affected if care is not taken to compare the confined material to the same material in the unconfined state, and both after removal of any residual monomer.

These issues are often recognized by researchers in the field, although some works simply report the $T_{\mathfrak{g}}$ of the bulk material and that of the nanoconfined polymer synthesized in the same conditions. For example, Mijangos and coworkers [82] report a 10 K increase in Tg for polystyrene synthesized in 35 nm AAO with the nanoconfined material having higher conversion, lower molecular weight, and higher syndiotacticity than the bulk, but they do note that only a 2 K difference was observed in their prior work when simply infiltrating polystyrene in this AAO, and hence, they attribute the slightly larger increase to the change in tacticity. In the case of a polymerizable ionic liquid containing a vinyl group on the butyl imidazolium cation investigated by Paluch and coworkers [129], two T_os were found for the material imbibed and polymerized in AAO, with Tg2 being higher than the bulk-synthesized polymer and independent of pore size, and Tg1 decreasing with pore size and being similar but slightly lower than that of the unpolymerized ionic liquid. In more recent work on a vinyl-octyl-imidazolium monomer [130], two T_gs were again observed and both increased as a result of the reaction by approximately 18 and 10 K, for RAFT and free radical polymerizations, respectively. However, in the latter work, although high molecular weight and low PDI polymers were made, conversions ranged from as low as 12-71%, and the T_gs of the reaction mixtures were not compared to those from bulk polymerizations.

7. Nanoconfined polymerizations: influence on thermal stability and conductivity

Nanoconfinement is also found to positively influence the thermal stability of polymers synthesized in confined environments. The thermal degradation of polystyrene (PS) polymerized in bulk and under nanoconfinement are compared in Fig. 18 from three research groups [82, 131,132]. Kitagawa and coworkers examined the degradation of polystyrene synthesized by free radical polymerization in PCP after extraction of the material by dissolving the PCP [131], and in particular, they compared the effect of pristine (unmodified) PCP and PCP functionalized with the crosslinking agent, 2,5-divinyl-terephthalate (DVTPA).

After completion of the polymerization, the crosslinked PS was found to be insoluble in common organic solvents, and its thermal stability from dynamic scans in thermogravimetric analysis (TGA) showed superior thermal stability compared with PS extracted from pristine PCP, as shown in Fig. 18. Polystyrene typically undergoes complete weight loss around 420 °C under nitrogen via the unzipping degradation mechanism, but the crosslinked material shows a two-step degradation with the second step at nearly 600 °C. Moreover, this was achieved with only 7 mol % crosslinking agent in the PCP which produced 45% primary char, compared to the conventional methodology which uses 40 mol % DVB [133] crosslinker to form a similar amount (40%) of primary char to elevate the degradation temperature up to 550 $^{\circ}\text{C}.$ Also shown in Fig. 18, the thermal stability of free radically-polymerized polystyrene nanoconfined in 35 nm AAO template is enhanced compared to that of bulk [82], as reflected by the shift of onset and peak values towards higher temperatures. In this case, the authors attribute the improved thermal stability of polymer plus AAO template to the high degree of syndiotactic character for the nanoconfined-polymerized PS, consistent with work from Vyazovkin and coworkers on the effect of tacticity on PS thermal stability [134].

The influence of nanoconfinement on thermal degradation of polystyrene has also been investigated using ellipsometry by Fakhraai and coworkers for 8000 g/mol films that were annealed to flow into the porous interstices of closely packed SiO₂ nanoparticles [132]. Thermal stability improves as the nanoparticle size decreases and the corresponding pore size associated with the interstitial space decreases. A two-step degradation mechanism is proposed, consisting of rapid mass loss at the free surface and the subsequent degradation of the PS confined in the nanopore interstitial space. In addition, the activation energy for thermal degradation increases 50 kJ/mol over the bulk value for 11 nm particles (3 nm pores), resulting in higher barrier under the more confined environment. The thermal degradation process is regarded as diffusion controlled, thus, nanoconfinement is capable of reducing the diffusivity of free radicals and oxygens to delay the degradation and the formation of char, suggesting its use in highly filled systems to improve flammability.

Nanoconfined polymerization followed by pyrolysis also improves the electronic properties of the graphitized nanowires produced. Both polyacrylonitrile (PAN) [135] and polyaniline (PANI) [136] under 3 nm confinement in MCM hosts show improved charge carrier properties compared to their bulk-polymerized counterparts due to the dipolar interaction between chain backbone and pore wall surface that orients the chains. The PAN-MCM composites have superior conductivity as pyrolysis temperature goes beyond 500 °C, reaching a microwave conductivity of 10^{-1} S/cm, ten times higher rather than bulk PAN at 1000 °C. Enhancement is attributed to larger domains of ordered carbon

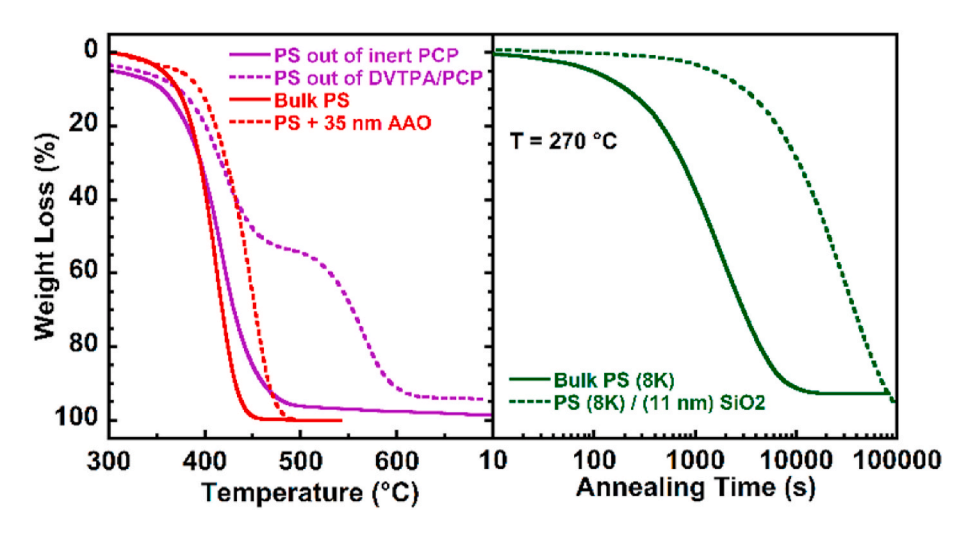


Fig. 18. Thermal degradation of bulk and nanoconfined polystyrene (PS) measured by TGA in dynamic mode under N₂ (left) and isothermally by spectroscopic ellipsometry in air (right). Purple solid lines represent PS extracted from pristine PCP channel and purple dashed line represent crosslinked PS extracted from crosslinker-functionalized PCP [131]. Red solid lines represent bulk PS and red dashed lines represent nanoconfined PS in the AAO template [82]. Green solid lines represent bulk PS and green dashed lines represent PS imbibed into the interstices of 11 nm packed SiO₂ nanoparticles [132]. (For interpretation of the references to color in this figure legend, the reader is referred to the Web version of this article.)

nanowire formed under the restricted MCM host channel. On the other hand, PANI-MCM composites only show a conductivity of 0.0014 S/cm, compared to 0.0057 S/cm for bulk PANI, with the conductivity increasing by a factor of four after the material is extracted from the MCM. In addition, dynamic TGA analysis shows that the pyrolytic graphitization of polyaniline in 3 nm MCM [136] is slowed down due to reduced diffusivity under nanoconfinement and shifts to higher temperatures (350–600 $^{\circ}$ C) compared with bulk PANI, which shows decomposition at 300–400 $^{\circ}$ C.

In another example but at larger nanopore sizes of 40 nm, a MOF template containing $FeCl_3$ as oxidant [137] is used to tune the electronic properties of poly(3,4-ethylenedioxythiophene) (PEDOT). A comparison between bulk synthesized PEDOT film and extracted nano-PEDOT reveals that extracted PEDOT had only marginal lower current for the same applied voltage than the bulk film indicating that nanoconfined films are high molecular weight products with semiconducting properties. However, the mechanical properties of nano-synthesized PEDOT is worse than the bulk, with Young's modulus for the extracted PEDOT being only one-fourth of bulk PEDOT, presumably due to the presence of nanoporosity in the PEDOT synthesized under nanoconfinement.

8. Nanocomposites as nanoreactors

As shown by Fakhraai and coworkers [132], the interstitial pores in packed nanoparticles can serve as a confined environment, albeit with the opposite curvature compared with nanoporous constraints. Conventional nanocomposites have much lower loadings of particles, and although the degree of confinement is lower than in the packed particle case, analogies have been made between nanocomposites and confined ultrathin polymer films [138-141] although they are not universally quantitative [142]. Several investigations [143-145] have been performed in which monomer is confined by and polymerized in the presence of graphite oxide (GO) nanofiller, which is known to improve mechanical, thermal, optical, and electrical properties [146,147]. In-situ polymerized GO nanocomposite using butyl methacrylate and benzoyl peroxide initiator show slightly enhanced molecular weight attributed to reduced initiator efficiency and a significantly increase in the degradation temperature from 320 $^{\circ}\text{C}$ for 80% weight loss in the bulk to approximately 380 °C for 3 wt % GO nanocomposites [143]. Similar results were found for GO polystyrene nanocomposites [144], as well as for a styrene/butyl methacrylate copolymer [145], with molecular weight monotonically increasing as GO filler content increases. Howopposite effect is observed with vinyl-functionalization of GO, where reductions in molecular weight increase significantly as functionalized GO content increases, seemingly due to termination of chains on the functionalized surface and/or due to reduction in monomer availability due to reaction with the surface. In the case of a crosslinkable polysulfide synthesized in-situ with both free and GO-surface functionalized chloropropyl crosslinking agent [146], both the nanocomposite Tg, its degree of crystallinity, and its thermal stability all increased with graphene content, reaching a maximum at 0.7 wt % functionalized GO. Similarly, $T_{\rm g}$ and thermal stability increase for a polystyrene nanocomposite with in-situ polymerization performed in the presence of functionalized clay [148].

In the nanocomposite synthesized by the in-situ step growth polymerization of cyanate ester [149], attapulgite (ATT) clay, a nanorod consisted of magnesium aluminum silicate with a pore size of 20 nm, the amine groups on the clay catalyze the reaction and also react with some of the monomer to form isourea and, thereby, reduce the crosslink density of the fully cured network. The result is a decrease in $T_{\rm g}$ by approximately 30 $^{\circ}{\rm C}$ for 8 wt % addition of ATT. In spite of this, the modulus and strength increased by 40% at 4 wt % ATT compared with bulk resin and the fracture toughness increased by 55% at this same clay loading.

9. Discussion

We have demonstrated from our own work and that in the literature that polymer synthesis using nanoreactors or under nanoconfinement is a powerful tool to produce polymers with properties that differ from the bulk. The changes in polymer properties result directly from changes in the kinetics of the nanoconfined polymerizations and several competing factors determine whether the kinetics are faster, slower, unchanged, or change as a function of conversion. These factors are i) layering or orientation of monomers or growing chains at the pore wall, resulting in changes in tacticity, for example, when the growing chain in free radical polymerization is oriented at the wall, and/or resulting in an increase in the local concentration of functional groups leading to increased reaction rates; ii) decreases in diffusivity which can lead to slower reaction rates and, in the case of free radical polymerization, can also lead to suppression of chain transfer to polymer, suppression of termination, and an earlier onset of autoacceleration; and iii) catalysis or inhibition effects cause by chemical moieties on the pore surface, e.g., hydroxyl groups on the native oxides or chemical groups added through functionalization of the surface. In several cases, the physics of these effects have been modeled by us and other groups and describe not only the changes in the reaction kinetics but also the changes in, for example, molecular weight and PDI.

Nanoconfinement can, thus, be used as a synthetic tool to tailor or engineer desired characteristics in polymeric products. However, as alluded to in the introduction, exploitation of this tool is a challenge because the polymer produced must be either extracted from conventional confinement matrix or the matrix must be dissolved requiring organic solvents or harsh chemicals, neither of which lend themselves to environmentally-friendly processing. Hence, novel nanoreactor platforms need to be created that facilitate the downstream separation and collection of the polymer product. Potential "green" nanoreactors may use soft confinement, for example nanoscale cylindrical jets of polymerizable monomer or nanoscale emulsions, that allow the polymeric product to be easily separated. Another alternative may be a nanoscale reactive extruder or a nanoreactor employing a hard confinement that can be reversibly softened or liquified under mild conditions.

10. Conclusion

In this review, we provided an overview of the literature dealing with nanoconfined liquid-state polymerization and the resulting properties of the synthesized polymers using primarily work from our laboratory as illustrative examples. The conventional confinement hosts, CPG, silica gel, AAO, and MOF or PCP were reviewed and their advantages and disadvantages for use as polymerization nanoreactors discussed. The changes in the reaction kinetics of nanoconfined free radical, step growth, and ring opening polymerizations depend on a number of competing factors, including layering or orientation of molecules at the pore surface, a decrease in molecular or segmental diffusivity, and catalytic or inhibition effects of chemical moieties on the pore surface, including hydroxyl groups on native oxides or expressly functionalized surfaces. Generally speaking, nanoconfinement tends to increase the rate of reaction and to produce polymers with higher molecular weight and a more ordered structure, but opposite results are also observed and cases vary depending on the monomer, reaction mechanism, and confinement type, size, and surface chemistry. Tg increases for poly (methyl methacrylate) and polystyrene synthesized in nanopores but decreases for polycyanurates, although care must be taken to ensure a fair comparison with the bulk in the case that the polymer product itself is different than that obtain in a bulk polymerization. In addition, thermal stability and conductivity of polymers synthesized under nanoconfinement improve. The prime disadvantage of nanoconfined polymerization is that of extraction of the polymer product, which currently is done by solvent extraction or matrix dissolution. This issue can be circumvented by in-situ nanocomposite polymerizations in which

the interstitial space between nanoparticles serves to confine the polymerization, but of course, this alternative only works if a nanocomposite material will suffice for the application at hand. Novel nanoreactor platforms are, thus, required that facilitate the downstream separation in order to fully exploit the use of nanoconfined polymerizations as a synthesis tool to engineer and tailor the properties of polymers.

Declaration of competing interest

The authors declare that they have no known competing financial interests or personal relationships that could have appeared to influence the work reported in this paper.

Acknowledgement

The authors gratefully acknowledge funding from NSF DMR 2004960.

References

- C.L. Jackson, G.B. McKenna, The glass-transition of organic liquids confined to small pores, J. Non-Cryst. Solids 131 (1991) 221–224.
- [2] C.L. Jackson, G.B. McKenna, Vitrfication and crystallization of organic liquids confined to nanoscale pores, Chem. Mater. 8 (1996) 2128–2137.
- [3] G. Liu, Y. Li, J. Jonas, Confined geometry-effects on reorientational dynamics of molecular liquids in porous silica glasses, J. Chem. Phys. 95 (9) (1991) 6902 6001
- [4] J.-Y. Park, G.B. McKenna, Size and confinement effects on the glass transition of polystyrene/O-terphenyl polymer solutions, Phys. Rev. B 61 (10) (2000) 6667–6676.
- [5] W. Zheng, S.L. Simon, Confinement effects on the glass transition of hydrogen bonded liquids, J. Chem. Phys. 127 (19) (2007) 194501/1–19450111.
- [6] J. Schüller, Y.B. Mel'nichenko, R. Richert, E.W. Fischer, Dielectric studies of the glass-transition in porous-media, Phys. Rev. Lett. 73 (1994) 2224–2227.
- [7] J. Schüller, R. Richert, E.W. Fischer, Dielectric relaxation of liquids at the surface of a porous glass, Phys. Rev. B 52 (1995) 15232–15238.
- [8] Y.B. Mel'nichenko, J. Schüller, R. Richert, B. Ewen, C.-K. Loong, Dynamics of hydrogen-bonded liquids confined to mesopores-A dielectric and neutron spectroscopy study, J. Chem. Phys. 103 (1995) 2016–2024.
- [9] M. Arndt, R. Stannarius, W. Gorbatschow, F. Kremer, Dielectric investigations of the dynamic glass transition in nanopores, Phys. Rev. E 54 (1996) 5377–5390.
- [10] P. Pissis, A. Kyritsis, D. Daoukaki, G. Barut, R. Pelster, G. Nimtz, Dielectric studies of glass transition in confined propylene glycol, J. Phys. Condens. Matter 10 (1998) 6205–6227.
- [11] J. Mattsson, J.A. Forrest, L. Borjesson, Quantifying glass transition behavior in ultrathin free-standing polymer films, Phys. Rev. E 62 (4) (2000) 5187–5200.
- [12] J.A. Forrest, J. Mattsson, Reductions of the glass transition temperature in thin polymer films: probing the length scale of cooperative dynamics, Phys. Rev. E. 61 (1) (2000) R53–R56.
- [13] J.A. Forrest, J. Mattsson, Using polymer films to probe finite size effects in glass forming materials, J. Phys. IV (P7) (2000) 251–254, 10.
- [14] D.S. Fryer, P.F. Nealey, J.J. de Pablo, Thermal probe measurements of the glass transition temperature for ultrathin polymer films as a function of thickness, Macromolecules 33 (2000) 6439–6447.
- [15] K. Fukao, Y. Miyamoto, Glass transition temperature and dynamics of alphaprocess in thin polymer films, Europhys. Lett. 46 (5) (1999) 649–654.
- [16] J.A. Forrest, K. Dalnoki-Veress, J.R. Dutcher, Interface and chain confinement effects on the glass transition temperature of thin polymer films, Phys. Rev. E 56 (1997) 5705–5716.
- [17] T. Kajiyama, K. Tanaka, A. Takahara, Surface thermomechanical and glass transition temperature measurements of polymeric solids, Macromol. Symp. 118 (1997) 677–682
- [18] G.B. DeMaggio, W.E. Frieze, D.W. Gidley, M. Zhu, H.A. Hristov, A.F. Yee, Interface and surface effects on the glass transition in thin polystyrene films, Phys. Rev. Lett. 78 (1997) 1524–1527.
- [19] J.A. Forrest, A.C. Rowat, K. Dalnoki-Veress, J.R. Stevens, J.R. Dutcher, Brillouin light scattering studies of the mechanical properties of polystyrene/polyisoprene multilayered thin films, J. Polym. Sci., Part B: Polym. Phys. 34 (17) (1996) 3009–3016.
- [20] J.A. Forrest, K. Dalnoki-Veress, J.R. Stevens, J.R. Dutcher, Effect of free surfaces on the glass transition temperature of thin polymer films, Phys. Rev. Lett. 77 (1996) 2002–2005.
- [21] J.L. Keddie, R.A.L. Jones, R.A. Cory, Size-dependent depression of the glasstransition temperature in polymer-films, Europhys. Lett. 27 (1994) 59–64.
- [22] O.K.C. Tsui, T.P. Russell, C.J. Hawker, Effect of interfacial interactions on the glass transition of polymer thin films, Macromolecules 34 (16) (2001) 5535–5539.
- [23] C.J. Ellison, S.D. Kim, D.B. Hall, J.M. Torkelson, Confinement and processing effects on glass transition temperature and physical aging in ultrathin polymer films: novel fluorescence measurements, Eur. Phys. J. E. 8 (2002) 155–166.

[24] J.A. Forrest, R.A.L. Jones, The glass transition and relaxation dynamics in thin polymer films, in: A. Karim, S. Kumar (Eds.), Polymer Surface Interfaces and Thin Films, World Scientific, Singapore, 2000.

- [25] J.A. Forrest, K. Dalnoki-Veress, The glass transition in thin polymer films, Adv. Colloid Interface Sci. 94 (1–3) (2001) 167–196.
- [26] M. Alcoutlabi, G.B. McKenna, Effects of confinement on material behaviour at the nanometre size scale, J. Phys. Condens. Matter 17 (2005) R461–R524.
- [27] C. Alba-Simionesco, B. Coasne, G. Dosseh, G. Dudzidak, K.E. Gubbins, R. Randhakrishnan, M. Silininska-Bartkowiak, Effects of confinement on freezing and melting, J. Phys. Condens. Matter 18 (2006) R15–R68.
- [28] C.B. Roth, J.R. Dutcher, Glass transition and chain mobility in thin polymer films, J. Electroanal. Chem. 584 (2005) 13–22.
- [29] H. Clasen, Polymerisation in einer Kanaleinschlussverbindung .1. Nachweis Am system dimethylbutadien-thioharnstoff, Zeitschrift fur Elektrochemie 60 (9–10) (1956) 982–987.
- [30] J.F. Brown Jr., D.M. White, Stereospecific polymerization in thiourea canal complexes, J. Am. Chem. Soc. 82 (21) (1960) 5671–5678.
- [31] D.M. White, Stereospecific polymerization in urea canal complexes, J. Am. Chem. Soc. 82 (21) (1960) 5678–5685.
- [32] F. Cataldo, O. Ursini, G. Angelini, P. Ragni, Radiation-induced inclusion polymerization of (-)Pinene in deoxycholic acid, J. Macromol. Sci., Pure Appl. Chem. 46 (5) (2009) 493–502.
- [33] F. Cataldo, O. Ursini, G. Angelini, Asymmetric radiation-induced inclusion polymerization of 3-methyl-1,4-pentadiene in deoxycholic acid, Radiat. Phys. Chem. 79 (1) (2010) 57–63.
- [34] H.R. Allcock, G.K. Dudley, E.N. Silverberg, Stereocontrolled polymerization of diene monomers within a tris (o-phenylenedioxy) cyclotriphosphazene tunnel clathrate, Macromolecules 27 (4) (1994) 1039–1044.
- [35] H.R. Allcock, E.N. Silverberg, G.K. Dudley, Stereocontrolled polymerization within a cyclophosphazene clathrate tunnel system, Macromolecules 27 (4) (1994) 1033–1038.
- [36] J.-T. Zou, Y.-S. Wang, W.-M. Pang, L. Shi, F. Lu, Radiation-induced inclusion polymerization of acrylonitrile in urea canals: toward synthesis of completely isotactic polyacrylonitrile with controlled molecular weight, Macromolecules 46 (5) (2013) 1765–1771.
- [37] W. Haller, Chromatography on glass of controlled pore size, Nature 206 (4985) (1965) 693.
- [38] T.R. Bryans, V.L. Brawner, E.L. Quitevis, Microstructure and porosity of silica xerogel monoliths prepared by the fast sol-gel method, J. Sol. Gel Sci. Technol. 17 (2000) 211.
- [39] A. Stein, B.J. Melde, R.C. Schroden, Hybrid inorganic-organic mesoporous silicates-nanoscopic reactors coming of age, Adv. Mater. 12 (19) (2000) 1403–1419
- [40] Z.A. ALOthman, A review: fundamental aspects of silicate mesoporous materials, Materials 5 (2012) 2874–2902.
- [41] R.K. Sharma, S. Sharma, S. Dutta, R. Zboril, M.B. Gawande, Silica-nanosphere-based organic-inorganic hybrid nanomaterials: synthesis, functionalization and applications in catalysis, Green Chem. 17 (6) (2015) 3207–3230.
- [42] C.T. Kresge, M. Leonowicz, W.J. Roth, J.C. Vartuli, J.S. Beck, Ordered mesoporous molecular sieves synthesized by a liquid-crystal template mechanism, Nature 359 (1992) 710–712.
- [43] J.S. Beck, J.C. Vartuli, W.J. Roth, M.E. Leonowicz, C.T. Kresge, K.D. Schmidt, C. T. Chu, D.H. Olson, E.W. Sheppard, S.B. McCullen, J.B. Higgens, J.L. Schlenker, A new family of mesoporous molecular-sieves prepared with liquid-crystal templates, J. Am. Chem. Soc. 114 (1992) 10834–10843.
- [44] D. Zhao, J. Feng, Q. Huo, N. Melosh, G.H. Fredrickson, B.F. Chemlka, G.D. Stucky, Triblock copolymer syntheses of mesoporous silica with periodic 50 to 300 angstrom pores, Science 279 (1998) 548–552.
- [45] P. Yang, D. Zhao, D.I. Margolese, B.F. Chmelka, G.D. Stucky, Generalized syntheses of large-pore mesoporous metal oxides with semicrystalline frameworks, Nature 396 (1998) 152–155.
- [46] B. Smarsly, C. Goeltner, M. Antonietti, W. Ruland, E. Hoinkis, SANS investigation of nitrogen sorption in porous silica, J. Phys. Chem. B 105 (2001) 831–840.
- [47] C.G. Goeltner, B. Smarsly, B. Berton, M. Antonietti, On the microporous nature of mesoporous molecular sieves, Chem. Mater. 13 (2001) 1617–1624.
- [48] K. Kageyama, J.-I. Tamazawa, T. Aida, Extrusion polymerization: catalyzed synthesis of crystalline linear polyethylene nanofibers within a mesoporous silica, Sci. 285 (24) (1999) 2113–2115.
- [49] X. Ji, J.E. Hampsey, Q. Hu, J. He, Z. Yang, Y. Lu, Mesoporous silica-reinforced polymer nanocomposites, Chem. Mater. 15 (2003) 3656–3662.
- [50] L.M. Wei, N.T. Hu, Y.F. Zhang, Synthesis of polymer–mesoporous silica nanocomposites, Materials 3 (2010) 4066–4079.
- [51] L. Wei, Y. Zhang, Emulsion polymerization of ethylene from mesoporous silica nanoparticles with vinyl functionalized monolayers, J. Polym. Sci., Polym. Chem. Ed. 47 (2009) 1393–1402.
- [52] K.-T. Li, C.-L. Dai, C.-Y. Li, Synthesis of linear low density polyethylene with a nano-sized silica supported Cp₂ZrCl₂/MAO catalyst, Polym. Bull. 64 (2010) 749–759.
- [53] M. MacLachlan, P. Aroca, N. Coombs, I. Manners, G.A. Ozin, Ring-opening polymerization of a [1]Silaferrocenophane within the channels of mesoporous silica: poly(ferrocenylsilane)-MCM-41 precursors to magnetic iron nanostructures, Adv. Mater. 10 (2) (1998) 144–149.
- [54] B. Yuan, X.H. He, Y.W. Chen, K.T. Wang, Preparation of nanosilica/ polynorbornene nanocomposite by covalently immobilized silica-supported acetylacetonate palladium(II) dichloride catalyst, Macromol. Chem. Phys. 212 (2011) 2378–2388.

- [55] W. Lee, S.J. Park, Porous anodic aluminum oxide: anodization and TemplatedSynthesis of functional nanostructures, Chem. Rev. 114 (2014) 7487–7556.
- [56] M. Pallaka, D. Unruh, S.L. Simon, Melting behavior of n-alkanes in anodic aluminum oxide (AAO) nanopores using Flash differential scanning calorimetry, Thermochim. Acta 663 (2018) 157–164.
- [57] T. Uemura, N. Yanai, S. Kitagawa, Polymerization reactions in porous coordination polymers, Chem. Soc. Rev. 38 (2009) 1228–1236.
- [58] T. Uemura, Y. Kadowaki, N. Yanai, S. Kitagawa, Template synthesis of porous polypyrrole in 3D coordination nanochannels, Chem. Mater. 21 (2009) 4096–4098.
- [59] T. Uemura, T. Kaseda, S. Kitagawa, Controlled synthesis of anisotropic polymer particles templated by porous coordination polymers, Chem. Mater. 25 (2013) 3772–3776.
- [60] H.Y. Zhao, S.L. Simon, Methyl methacrylate polymerization in nanoporous confinement, Polymer 52 (2011) 4093–4098.
- [61] F. Begum, H.Y. Zhao, S.L. Simon, Modeling methyl methacrylate free radical polymerization: reaction in hydrophobic nanopores, Polymer 53 (15) (2012) 3261–3268.
- [62] F. Begum, H.Y. Zhao, S.L. Simon, Modeling methyl methacrylate free radical polymerization: reaction in hydrophilic nanopores, Polymer 53 (15) (2012) 3238, 3244
- [63] Q. Tian, H.Y. Zhao, S.L. Simon, Kinetic study of alkyl methacrylate polymerization in nanoporous confinement over a broad temperature range, Polymer 205 (2020) 122868/1–9.
- [64] H.Y. Zhao, S.L. Simon, Equilibrium free-radical polymerization of methyl methacrylate under nanoconfinement, Polymer 66 (2015) 173–178.
- [65] H.Y. Zhao, Z.N. Yu, F. Begum, R.C. Hedden, S.L. Simon, The effect of nanoconfinement on methyl methacrylate polymerization: T_g, molecular weight, and tacticity, Polymer 55 (2014) 4959–4965.
- [66] G.D. Verros, T. Latsos, D.S. Achilia, Development of a unified framework for calculating molecular weight distribution in diffusion controlled free radical bulk homo-polymerization Polymer, Polymer 46 (2) (2005) 539–552.
- [67] T. Cui, J. Ding, J.Z.Y. Chen, Dynamics of a self-avoiding polymer chain in slit, tube, and cube confinements, Phys. Rev. 78 (6) (2008), 061802/1-7.
- [68] K. Avramova, A. Milchev, Polymer chains in a soft nanotube: a Monte Carlo study, J. Chem. Phys. 124 (2) (2006), 024909/1-8.
- [69] C. H. Zhai and S. L. Simon, (unpublished data).
- 170 T. Uemura, Y. Ono, K. Kitagawa, S. Kitagawa, Radical polymerization of vinyl monomers in porous coordination polymers: nanochannel size effects on reactivity, molecular weight, and stereostructure, Macromolecules 41 (2008) 87–94.
- [71] S.M. Ng, S.-I. Ogino, T. Aida, Free radical polymerization within mesoporous zeolite channels, Macromol. Rapid Commun. 18 (1997) 991–996.
- [72] X. Xu, Y.N. Zeng, C.L. Yu, F. Zhang, Controlled RAFT polymerization of MMA in confined space of various pore sizes of SBA-15, J. Porous Mater. 27 (2020) 95–105.
- [73] I.M. Kalogeras, E.R. Neagu, Interplay of surface and confinement effects on the molecular relaxation dynamics of nanoconfined poly(methyl methacrylate) chains, Eur. Phys. J. E 14 (2004) 193–204.
- [74] X.C. Li, T.A. King, F. Pallikari-Viras, Characteristics of composites based on PMMA modified gel silica glasses, J. Non-Cryst. Solids 170 (1994) 243–249.
- [75] F. Pallikari-Viras, X.C. Li, T.A. King, Thermal analysis of PMMA/gel silica glass composites, J. Sol. Gel Sci. Technol. 7 (1996) 203–209.
- [76] M. Michailidis, G.D. Verros, E.A. Deliyanni, E.G. Andriotis, D.S. Achilias, An experimental and theoretical study of butyl methacrylate in situ radical polymerization kinetics in the presence of graphene oxide nanoadditives, J. Polym. Sci., Polym. Chem. Ed. 55 (8) (2017) 1433–1441.
- \cite{Model} Q. Tian and S. L. Simon, unpublished data 2020.
- [78] M. Lazár, L. Hrčková, A. Fiedlerova, E. Borsig, Crosslinking during radical polymerization of dodecyl methacrylate, Macromol. Mater. Eng. 283 (1) (2000) 88–92.
- [79] M. Lazár, L. Hrčková, E. Borsig, Polymerization of n-dodecyl methacrylate into high conversion, J. Macromol. Sci., Part A 39 (5) (2002) 365–377.
- [80] R.K. Graham, Gamma irradiation of poly(alkyl methacrylates), J. Polym. Sci. 38 (3) (1959) 209–212.
- [81] J. Barton, Peroxide Crosslinking of Poly(n-alkyl methacrylates), J. Polym. Sci. 1 Polym. Chem. 6 (1968) 1315–1323.
- [82] J.M. Giussi, I. Blaszczyk-Lezak, M.S. Cortizo, C. Mijangos, In-situ polymeirzaiton of styrene in AAO nanocavities, Polymer 54 (2013) 6886–6893.
- [83] H.C. Lee, J. Hwang, U. Schilde, M. Antonietti, K. Matyjaszewski, B.V.K. J. Schmidt, Toward ultimate control of radical polymerization: functionalized metal—organic frameworks as a robust environment for metal-catalyzed polymerizations, Chem. Mater. 30 (2018) 2983–2994.
- [84] J. Hwang, H.C. Lee, M. Antonietti, B.V.K.J. Schmidt, Free radical and raft polymerization of vinyl esters in metal-organic-frameworks, Polym. Chem. 8 (2017) 6204.
- [85] T. Kitayama, O. Nakagawa, K. Hatada, Stereospecific polymerization of stereoregular poly (methyl methacrylate) macromonomer and determination of main-chain tacticity of resulting polymacromonomer, Polym. J. 28 (1) (1996) 150-154
- [86] Y. Isobe, K. Yamada, T. Nakano, Y. Okamoto, Stereospecific free-radical polymerization of methacrylates using fluoroalcohols as solvents, Macromolecules 32 (18) (1999) 5979–5981.

[87] Y. Isobe, K. Yamada, T. Nakano, Y. Okamoto, Stereocontrol in the free-radical polymerization of methacrylates with fluoroalcohols, J. Polym. Sci., Polym. Chem. Ed. 38 (S1) (2000) 4693–4703.

- [88] A. Matsumoto, S. Nakamura, Radical polymerization of methyl methacrylate in the presence of magnesium bromide as the Lewis acid, J. Appl. Polym. Sci. 74 (2) (1999) 290–296.
- [89] Y. Isobe, T. Nakano, Y. Okamoto, Stereocontrol during the free-radical polymerization of methacrylates with Lewis acids, J. Polym. Sci., Polym. Chem. Ed. 39 (9) (2001) 1463–1471.
- [90] T. Uemura, Y. Ono, Y. Hijikata, S. Kitagawa, Functionalization of coordination nanochannels for controlling tacticity in radical vinyl polymerization, J. Am. Chem. Soc. 132 (13) (2010) 4917–4924.
- [91] S. Amanuel, V.M. Malhotra, Effects of physical confinement (< 125 nm) on the curing behavior of phenolic resin, J. Appl. Polym. Sci. 99 (6) (2006) 3183–3186.
- [92] E. Lopez, S.L. Simon, Trimerization reaction kinetics and Tg depression of polycyanurate under nanoconfinement, Macromolecules 48 (13) (2015) 4692–4701.
- [93] Y.P. Koh, S.L. Simon, Kinetic study of trimerization of monocyanate ester in nanopores, J. Phys. Chem. B 115 (5) (2011) 925–932.
- [94] Y.P. Koh, S.L. Simon, Trimerization of monocyanate ester in nanopores, J. Phys. Chem. B 114 (23) (2010) 7727–7734.
- [95] Y.P. Koh, Q.X. Li, S.L. Simon, T_g and reactivity at the nanoscale, Thermochim. Acta 492 (1–2) (2009) 45–50.
- [96] Q.X. Li, S.L. Simon, Surface chemistry effects on the reactivity and properties of nanoconfined bisphenol M dicyanate ester/polycyanurate in controlled pore glass, Macromolecules 42 (10) (2009) 3573–3579.
- [97] Q.X. Li, S.L. Simon, Curing of bisphenol M dicyanate ester under nanoscale constraint, Macromolecules 41 (4) (2008) 1310–1317.
- [98] S.L. Simon, J.K. Gillham, Cure kinetics of a liquid dicyanate ester monomer/hightg polycyanurate material, J. Appl. Polym. Sci. 47 (3) (1993) 461–485.
- [99] M. Malvaldi, S. Bruzzone, F. Picchioni, Confinement effect in diffusion-controlled stepwise polymerization by Monte Carlo simulation, J. Phys. Chem. B 110 (2006) 12281–12288, 2006.
- [100] P.H. Lin, S. Kohale, R. Khare, Effect of nano-confinement on kinetics of cross-linking reactions: a molecular simulation study, J. Phys. Chem. B 115 (2011) 12348–12355.
- [101] B. Yancey, S. Vyazovkin, Venturing into kinetics and mechanism of nanoconfined solid-state reactions: trimerization of sodium dicyanamide in nanopores, Phys. Chem. Chem. Phys. 16 (2014) 11409.
- [102] B. Yancey, S. Vyazovkin, The kinetics and mechanism of nanoconfined molten salt reactions: trimerization of potassium and rubidium dicyanamide, Phys. Chem. Chem. Phys. 17 (2015) 10209.
- [103] M. Tarnacka, M. Dulski, S. Starzonek, K. Adrjanowicz, E.U. Mapesa, K. Kaminski, M. Paluch, Following kinetics and dynamics of DGBBA-aniline polymerization in nanoporous native alumina oxide membranes FTIR and dielectric studies, Polymer 68 (2015) 253–261.
- [104] G. Wissanrakkit, J.K. Gillham, The glass transition temperature (Tg) as an index of chemical conversion for a high-tg amine/epoxy system: chemical and diffusion controlled reaction kinetics, J. Coating Technol. 82 (783) (1990) 35–50.
- [105] S.L. Simon, J.K. Gillham, Reaction kinetics and TTT cure diagrams for offstoichiometric ratios of a high-tg epoxy/amine system, J. Appl. Polym. Sci. 46 (7) (1992) 1245–1270.
- [106] A.A. Tsyganenko, P.P. Mardilovich, Structure of alumina surfaces, J. Chem. Soc., Faraday Trans. 92 (23) (1996) 4843–4852.
- [107] H.A. Al-Abadleh, V.H. Grassian, FT-IR study of water adsorption on aluminum oxide surfaces, Langmuir 19 (2003) 341–347.
- [108] P.J. Eng, T.P. Trainor, G.E. Brown Jr., G.A. Waychunas, M. Newville, S.R. Sutton, M.L. Rivers, Structure of the hydrated α-Al₂O₃ (0001) surface, Science 288 (5468) (2000) 1029–1033.
- [109] K.C. Hass, W.F. Schneider, A. Curioni, W. Andreoni, The chemistry of water on alumina surfaces: reaction dynamics from first principles, Science 282 (5387) (1998) 265–268.
- [110] B. Sanz, N. Ballard, A. Marcos-Fernandez, J.M. Asua, C. Mijangos, Confinement effects in the step-growth polymerization within AAO templates and modeling, Polymer 140 (2018) 131–139.
- [111] M. Vaddey, M.S. Thesis, Nanoconfined Ring-Opening Metathesis Polymerization of Dicyclopentadiene, Texas Tech University, 2011.
- [112] E. Rabinowitch, Collision, Co-ordination, diffusion and reaction velocity in condensed systems, Trans. Faraday Soc. 33 (1937) 1225–1233.
- [113] K. Chen, M.A. Susner, S. Vyazovkin, Effect of the brush structure on the degradation mechanism of polystyrene-clay nanocomposites, Macromol. Rapid Commun. 26 (9) (2005) 690–695.
- [114] M. Tarnacka, A. Dzienia, P. Maksym, A. Talik, A. Zięba, R. Bielas, K. Kaminski, M. Paluch, Highly efficient ROP polymerization of ε-caprolactone catalyzed by nanoporous alumina membranes. How the confinement affects the progress and product of ROP reaction, Macromolecules 51 (2018) 4588–4597.
- [115] J.E. Pye, C.B. Roth, Two simultaneous mechanisms causing glass transition temperature reductions in high molecular weight freestanding polymer films as measured by transmission ellipsometry, Phys. Rev. Lett. 107 (23) (2011) 235701.
- [116] J.E. Pye, C.B. Roth, Above, below, and in-between the two glass transitions of ultrathin free-standing polystyrene films: thermal expansion coefficient and physical aging, J. Polym. Sci. B Polym. Phys. 53 (1) (2015) 64–75.
- [117] E.C. Glor, G.V. Angrand, Z. Fakhraai, Exploring the broadening and the existence of two glass transitions due to competing interfacial effects in thin, supported polymer films, J. Chem. Phys. 146 (20) (2017) 203330.

- [118] C.J. Ellison, J.M. Torkelson, The distribution of glass transition temperatures in nanoscopically confined glass formers, Nat. Mater. 2 (10) (2003) 695–700.
- [119] J.E. Pye, K.A. Rohald, E.A. Baker, C.B. Roth, Physical aging in ultrathin polystyrene films: evidence of a gradient in dynamics at the free surface and its connection to the glass transition temperature reductions, Macromolecules 43 (19) (2010) 8296–8303.
- [120] D. Kawaguchi, K. Tanaka, T. Kajiyama, A. Takahara, S. Tasaki, Mobility gradient in surface region of monodisperse polystyrene films, Macromolecules 36 (4) (2003) 1235–1240.
- [121] J.A. Forrest, J.S. Sharp, Free surfaces cause reductions in the glass transition temperature of thin polystyrene films, Phys. Rev. Lett. 91 (23) (2003) 235701.
- [122] S. Napolitano, C. Capponi, B. Vanroy, Glassy dynamics of soft matter under 1D confinement: How irreversible adsorption affects molecular packing, mobility gradients and orientational polarization in thin films, European Physical Journal E 36 (6) (2013), 61.
- [123] Y.C. Jean, J.J. Zhang, H.M. Chen, Y. Li, G. Liu, Positron annihilation spectroscopy for surface and interface studies in nanoscale polymeric films, Spectrochim. Acta, Part A 61 (2005) 1683–1691.
- [124] X.Y. Lang, Y.F. Zhu, Q. Jiang, Size and interface effects on several Kientic and thermodynamic properties of polymer thin films, Thin Solid Films 515 (2006) 2765–2770.
- [125] T. Miyazaki, K. Nishida, T. Kanaya, Thermal expansion behavior of ultrathin polymer films supported on silicon substrate, Phys. Rev. E 69 (2004), 061803.
- [126] J.L. Keddie, R.A.L. Jones, R.A. Cory, Interface and surface effects on the glasstransition temperature in thin polymer-films, Faraday Discuss 98 (1994) 219–230
- [127] D.S. Fryer, R.D. Peters, E.J. Kim, J.E. Tomaszewski, J.J. de Pablo, P.F. Nealey, C. C. White, W.L. Wu, Dependence of the glass transition temperature of polymer films on interfacial energy and thickness, Macromolecules 34 (16) (2001) 5627–5634.
- [128] N.B. Tito, J.E.G. Lipson, S.T. Milner, Lattice model of mobility at interfaces: free surfaces, substrates, and bilayers, Soft Matter 9 (39) (2013) 9403–9413.
- [129] M. Tarnacka, A. Chrobok, K. Matuszek, S. Golba, P. Maksym, K. Kaminski, M. Paluch, Polymerization of monomeric ionic liquid confined within uniaxial alumina pores as a new way of obtaining materials with enhanced conductivity, ACS Appl. Mater. Interfaces 8 (2016) 29779–29790.
- [130] P. Maksym, M. Tarnacka, A. Dzienia, K. Wolnica, M. Dulski, K. Erfurt, A. Chrobok, A. Zieba, A. Brzozka, G. Sulka, R. Bielas, K. Kaminski, M. Paluch, Efficient metalfree strategies for polymerization of a sterically hindered ionic monomer through the application of hard confinement and high pressure, RSC Adv. 9 (2019) 6396–6408.
- [131] G. Distefano, H. Suzuki, M. Tsujimoto, S. Isoda, S. Bracco, A. Comotti, P. Sozzani, T. Uemura, S. Kitagawa, Highly ordered alignment of a vinyl polymer by hostguest cross-polymerization, Nat. Chem. 5 (2013), 335-34.
- [132] H. Wang, Y. Qiang, A.A. Shamsabadi, P. Mazumder, K.T. Turner, L. Daeyeon, Z. Fakhraai, Thermal degradation of polystyrene under extreme nanoconfinement, ACS Macro Lett. 8 (11) (2019) 1413–1418.
- [133] G.F. Levchik, S. Kun, S.V. Levchik, G. Camino, C.A. Wilkie, The correlation between cross-linking and thermal stability: cross-linked polystyrenes and polymethacrylates, Polym. Degrad. Stabil. 65 (3) (1999) 395–403.

- [134] K. Chen, K. Harris, S. Vyazovkin, Tacticity as a factor contributing to the thermal stablity of polystyrene, Macromol. Chem. Phys. 208 (2007) 2525–2532.
- [135] C.G. Wu, T. Bein, Conducting carbon wires in ordered, nanomether-sized channels, Sci. 266 (5187) (1994) 1013–1015.
- [136] C.G. Wu, T. Bein, Conducting polyaniline filaments in a mesoporous channel host, Sci. 264 (5166) (1994) 1757–1759.
- [137] T. Wang, M. Farajollahi, S. Henke, T. Zhu, S.R. Bajpe, S. Sun, J.S. Barnard, J. S. Lee, J.D.W. Madden, A.K. Cheetham, S.K. Smoukov, Functional conductive nanomaterials via polymerization in nano-channels: PEDOT in a MOF, Mater. Horiz. 4 (1) (2017) 64–71.
- [138] F.W. Starr, T.B. Schroder, S.C. Glotzer, Effects of a nanoscopic filler on the structure and dynamics of a simulated polymer melt and the relationship to ultrathin films, Phys. Rev. E 64 (2001), 021802.
- [139] A. Bansal, H. Yang, C. Li, K. Cho, B.C. Benicewicz, S.K. Kumar, L.S. Schadler, Quantitative equivalence between polymer nanocomposites and thin polymer films, Nat. Mater. 4 (2005) 693–698.
- [140] A. Bansal, H. Yang, C. Li, B.C. Benicewicz, S.K. Kumar, L.S. Schadler, Controlling the thermormechanical properties of polymer nanocomposites by tailoring the polymer-particle interface, J. Polym. Sci., Part B: Polym. Phys. 44 (20) (2006) 2944–2950.
- [141] P. Rittigstein, J.M. Torkelson, Polymer-nanoparticle interfacial interactions in polymer nanocomposites: confinement effects on glass transition temperature and suppression of physical aging, J. Polym. Sci. B Polym. Phys. 44 (2006) 2935–2943.
- [142] J.M. Kropka, V. Pryamitsyn, V. Ganesan, Relation between glass transition temperatures in polymer nanocomposites and polymer thin films, Phys. Rev. Lett. 101 (7) (2008), 075702.
- [143] I. Tsagkalias, V. Proskynitopouloua, G. Verros, D.S. Achilias, Effect of graphene oxide on the kinetics of the radical polymerization of styrene, Mater. Today: Proceedings 5 (2018) 27517–27525.
- [144] I.S. Tsagkalias, A. Vlachou, G.D. Verros, D.S. Achilias, Effect of graphene oxide or functionalized graphene oxide on the copolymerization kinetics of styrene/nbutyl methacrylate, Polymers 11 (6) (2019) 999.
- [145] M. Amangah, M. Salami-Kalajahi, H. Roghani-Mamaqani, Nanoconfinement effect of graphene on thermophysical properties and crystallinity of matrixgrafted graphene/crosslinked polysulfide polymer nanocomposites, Diam. Relat. Mater. 83 (2018) 177–183.
- [146] H. Kim, A.A. Abdala, C.W. Macosko, Graphene/polymer nanocomposites, Macromolecules 43 (16) (2010) 6515–6530.
- [147] S. Park, R.S. Ruoff, Chemical methods for the production of graphenes, Nat. Nanotechnol. 4 (2009) 217–224.
- [148] S. Vyazovkin, I. Dranca, X. Fan, R. Advincula, Degradation and relaxation kinetics of Polystyrene—Clay nanocomposite prepared by surface initiated polymerization, J. Phys. Chem. B 108 (2004) 11672–11679.
- [149] Y. Pan, Y. Xu, L. An, H. Lu, Y. Yang, W. Chen, S. Nutt, Hybrid network structure and mechanical properties of rodlike silicate/cyanate ester nanocomposites, Macromolecules 41 (23) (2008) 9245–9258.